
Interpretable Machine Learning for Survival Analysis

Sophie Hanna Langbein^{1,2} | Mateusz Krzyżiński⁴ |
Mikołaj Spytek⁴ | Hubert Baniecki^{4,5} | Przemysław
Biecek^{4,5} | Marvin N. Wright^{1,2,3}

¹Leibniz Institute for Prevention Research and Epidemiology – BIPS, Bremen, Germany

²Faculty of Mathematics and Computer Science, University of Bremen, Germany

³Department of Public Health, University of Copenhagen, Denmark

⁴Faculty of Mathematics and Information Science, Warsaw University of Technology, Poland

⁵Faculty of Mathematics, Informatics and Mechanics, University of Warsaw, Poland

Correspondence

Marvin N. Wright, Leibniz Institute for Prevention Research and Epidemiology – BIPS, Bremen, Germany
Email: wright@leibniz-bips.de

Funding information

German Research Foundation (DFG), Grant Numbers: 437611051, 459360854

With the spread and rapid advancement of black box machine learning models, the field of interpretable machine learning (IML) or explainable artificial intelligence (XAI) has become increasingly important over the last decade. This is particularly relevant for survival analysis, where the adoption of IML techniques promotes transparency, accountability and fairness in sensitive areas, such as clinical decision making processes, the development of targeted therapies, interventions or in other medical or healthcare related contexts. More specifically, explainability can uncover a survival model's potential biases and limitations and provide more mathematically sound ways to understand how and which features are influential for prediction or constitute risk factors. However, the lack of readily available IML methods may have deterred medical practitioners and policy makers in public health from leveraging the full potential of machine learning for predicting time-to-event data. We present a comprehensive review of the limited existing amount of work on IML methods for survival analysis within the context of the general IML taxonomy. In addition, we formally detail how commonly used IML methods, such as such as individual conditional expectation (ICE), partial dependence plots (PDP), accumulated local effects (ALE), different feature importance measures or Friedman's H-interaction statistics can be adapted to survival outcomes. An application of several IML methods to real data on data on under-5 year mortality of Ghanaian children from the Demographic and Health Surveys (DHS) Program serves as a tutorial or guide for researchers, on how to utilize the techniques in practice to facilitate understanding of model decisions or predictions.

1 | INTRODUCTION

Survival analysis is a statistical subfield which analyzes and interprets time-to-event data, i.e. examining the duration until an event of interest (e.g., death, failure) occurs in a study population, while considering the effects of censoring. Censoring refers to the event of interest not being observed for some subjects before the study is terminated. For an extensive period of time, classic parametric and semi-parametric statistical methods, exemplified by the Cox proportional hazards model¹, have held a pervasive influence over the field of survival analysis. This dominance is largely attributable to their ability to handle censored data and yield reliable inferences in the form of hazard ratios. Hazard ratios are widely considered interpretable, clarifying underlying event dynamics, rendering the Cox proportional hazards model an indispensable tool in diverse scientific domains, including epidemiology, medicine, and engineering. However, in practice, the strong assumptions of the Cox model are often not met², with the noncollapsibility problem potentially leading to biased crude hazard ratio estimates³. In recent years, the ease of interpretability of the hazard ratio, which is readily assumed by a majority of domains regularly applying the Cox proportional hazard model, has been called into question, even under the condition that all basic Cox model assumptions are met⁴. Challenges of classical statistical methods such as the Cox model are amplified by the rapid development of big data technologies, leading to the collection of a wide variety and volume of survival data in many different disciplines. In this light, machine learning models prove a viable alternative to classic statistical models, due to their enhanced prediction performance and flexibility, especially when using high-dimensional, large datasets⁵. Popular machine learning survival models include survival tree ensemble methods^{6,7}, such as random survival forests and boosted trees, and survival neural networks^{8,9,10}.

While there is considerable promise in using machine learning models for survival analysis, the inherent opacity of black-box models has prompted legitimate concerns, since in fields such as the life sciences, results and model outputs must be interpretable to provide a solid basis for highly sensitive decision-making.^{11,12} This lack of interpretability may render it problematic to downright impossible to identify and understand the influence of specific risk factors on survival. There are further increasingly high regulatory standards for decisions made by artificial intelligence in a healthcare or biomedical context, which survival applications predominantly focus on. For instance, the European General Data Protection Regulation (GDPR), emphasizes the importance of transparency and accountability in the processing of personal data, in particular granting patients the right to understand how and why certain diagnoses or recommendations are made by artificial intelligence¹². Moreover, biases in survival data are easily concealed, even though they may adversely impact the analysis and decision making especially in medical domains, which may unfairly affect the patients in minority groups.^{13,14} Specifically for common survival analysis data, models and methods, recent papers have proven the existence unintentional biases toward protected attributes such as age, race, gender, and/or ethnicity.^{15,16,17} Research has shown that censoring is oftentimes not independent of protected attributes (e.g. marginalized minority groups often experience high exposure to censoring), potentially leading to an overestimation of survival predictions.^{18,19,20} All of these issues can be addressed by means of interpretable machine learning or explainable artificial intelligence methods.^{21,22}

So far, there are few interpretable machine learning methods applicable to or specifically developed for complex survival models. In general, the taxonomy of explanation methods divides interpretable machine learning methods into six different groups. The most important differentiation is between local and global methods, model-specific and model-agnostic methods, and post-hoc methods and ante-hoc interpretable models. In their most basic form, the most important local model-agnostic interpretability methods have been adapted to survival analysis, this includes *SurvLIME*²³, *SurvSHAP*²⁴ and *SurvSHAP(t)*²¹ and survival counterfactual explanations²⁵. Moreover, some specialized model-agnostic approaches, like *SurvNAM*²⁶ or *UncSurvEx*²⁷ have been developed, parallel to a set of interpretable machine learning survival models^{28,29,30,31}. While there are some reviews for explainable artificial intelligence in healthcare^{32,33,34}, we are not aware of any review specifically for survival analysis. Moreover, many foundational interpretable machine learning techniques, widely utilized in traditional settings have not yet been formally adapted to survival analysis.

The paper is structured into three main parts to address the aforementioned concerns. The first focus of the paper lies on a non-comprehensive, focus-driven review of all relevant contributions to survival interpretable machine learning, with a particular emphasis on model-agnostic explainability methods. Existing contributions are examined on a conceptual level, with attention directed toward their limitations with respect to real-world data and applications. The second focus of the paper is to mathematically and conceptually translate a set of fundamental interpretable machine learning methods from the classic machine learning setting to survival analysis. For model-agnostic local methods, this encompasses individual conditional expectation curves, while global model-agnostic methods are comprised of partial dependence curves, accumulated local effects, Friedman's H-statistic for feature interaction, permutation feature importance, conditional feature importance, leave-one-covariate-out, and functional decomposition methods. The third and final focus is put on providing a tutorial that showcases both existing and newly adapted methods using real-world data on under-5-year mortality of children in Ghana from the US Agency of International Development. The tutorial aims to guide practitioners in utilizing interpretability methods to elucidate the opaque mechanisms of black-box machine learning survival models and gain a broader perspective on interpretation beyond simple survival curves and hazard ratios, also for classical statistical models.

1.1 | Notation and Key Concepts of Survival Analysis

The objective of survival analysis is to model the time to an event of interest t given a set of training data D . In the standard right-censored setting, the training set D consists of n triplets $(\mathbf{x}^i, \delta^i, t^i)_{i=1}^n$, where $\mathbf{x}^i = (x_1^i, \dots, x_p^i)^T$ is a vector of the p covariates or features. We refer to a specific, undefined feature as $j = \{1, \dots, p\}$. If a selected instance i is observed, t^i represents the true duration between the baseline time and the event occurrence for that instance and the censoring indicator δ^i takes the value 1. In contrast, if the event is not observed, t^i signifies the time elapsed between the baseline time until either until the end of the observation period or until time of dropout and the true time to event is not observed. Then $\delta^i = 0$ is indicating a censored observation. The set of observed times to event is defined as $\{t_{n0}, \dots, t_n\}$; the ordered, unique, observed times to event are $\{t_0, \dots, t_m\}$. In the following, we refer to a specific undefined time to event as $t_s = t$ (when possible the index is dropped for notational convenience), the corresponding random variable is denoted as T .

Event time distributions are usually described by a set of common functions, such as survival or hazard functions. We generalize them as $f : \{\mathcal{X}, \mathcal{T}\} \rightarrow \mathbb{R}$, a set of functions that map value combinations from the feature space \mathcal{X} and the time space \mathcal{T} to a one-dimensional outcome. The survival function $f^S(t|\mathbf{x}) = \mathbb{P}(T > t|\mathbf{x})$ gives the probability of surviving beyond a specific timepoint t . The hazard function $f^h(t)$ describes the instantaneous rate of occurrence of the event of interest at a specific time t , given that no event occurred before time t . If $f^{pd}(t|\mathbf{x})$ is the probability density function of the event of interest, for which $f^{pd}(t|\mathbf{x}) = -\frac{df^S(t|\mathbf{x})}{dt}$ holds, then $f^h(t|\mathbf{x})$ is defined as

$$f^h(t|\mathbf{x}) = \lim_{\Delta t \rightarrow 0} \frac{\mathbb{P}(t \leq T \leq t + \Delta t | T \geq t, \mathbf{x})}{\Delta t} = \frac{f^{pd}(t|\mathbf{x})}{f^S(t|\mathbf{x})} = -\frac{d}{dt} \ln f^S(t|\mathbf{x}). \quad (1)$$

The integral of the hazard function up to a specific point in time t is the cumulative hazard function (CHF) $f^{\text{CHF}}(t|\mathbf{x})$. It represents the cumulative risk of experiencing the event of interest up to a specific time t , i.e.

$$f^{\text{CHF}}(t|\mathbf{x}) = \int_0^t f^h(z|\mathbf{x}) dz. \quad (2)$$

Using the hazard function and the CHF, the survival function can be expressed as

$$f^S(t|\mathbf{x}) = \mathbb{P}(T > t|\mathbf{x}) = \exp\left(-\int_0^t f^h(z|\mathbf{x}) dz\right) = \exp(-f^{\text{CHF}}(t|\mathbf{x})). \quad (3)$$

The Cox regression model¹ defines the survival function $f^S(t|\mathbf{x}, \mathbf{b})$ and the hazard function $f^h(t|\mathbf{x}, \mathbf{b})$ at time t given a set of features \mathbf{x} as:

$$f^S(t|\mathbf{x}, \mathbf{b}) = (f_0^S(t))^{\exp(\varphi(\mathbf{x}, \mathbf{b}))} = \exp(-f_0^h(t)) \exp(\varphi(\mathbf{x}, \mathbf{b})) \quad (4)$$

$$f^h(t|\mathbf{x}, \mathbf{b}) = f_0^h(t) \exp(\varphi(\mathbf{x}, \mathbf{b})) \quad (5)$$

$$\varphi(\mathbf{x}, \mathbf{b}) = \mathbf{b}^\top \mathbf{x} = \sum_{j=1}^p b_j x_j. \quad (6)$$

Here $\mathbf{b}^\top = (b_1, \dots, b_p)$ is an unknown vector of regression coefficients, $f_0^S(t)$ is the baseline survival function and $f_0^h(t)$ the baseline hazard function. Key properties of the Cox model are the linearity of the function $\varphi(\mathbf{x}, \mathbf{b})$ and its independence of time, as well as the independence of $f_0^h(t)$ and $f_0^S(t)$ from \mathbf{x} and \mathbf{b} .

2 | REVIEW OF INTERPRETABLE MACHINE LEARNING (IML) METHODS

2.1 | Local Methods

2.1.1 | Individual Conditional Expectation (ICE)

Originally introduced by Goldstein et al.³⁵, individual conditional expectation (ICE) curves visualize changes in prediction for one observation induced by feature changes. So far, they have not yet been formally adapted to survival data applications, which we present in the following. To formally define the ICE curves, let $A \subset \{1, \dots, p\}$ be the features of interest and let $-A$ be the complement set of A . The function predicted by the survival machine learning model is denoted as $\hat{f}(\cdot)$. For each observation, the feature matrix \mathbf{X} is partitioned into \mathbf{X}_A and \mathbf{X}_{-A} . For notational convenience in the following we will assume a single feature of interest, i.e. $|A| = 1$, which is also the most common setting for visualization purposes. To obtain the ICE curves a set of grid values $\mathbf{x}_A^{\text{grid}} = \{x_A^1, \dots, x_A^g\}$ is defined, at which, for every $i = 1, \dots, n$:

$$\hat{f}_{\text{ICE},A}^i(t|\mathbf{x}_A) = \hat{f}(t|\mathbf{x}_A^{\text{grid}}, \mathbf{x}_{-A}^i), \quad (7)$$

such that a set of $\{1, \dots, g\}$ ordered pairs is obtained: $\{(x_A^k, \hat{f}_A^i(t|x_A^k))\}_{k=1}^g$ for a fixed t .

Common choices for grid values are equidistant grid values within feature range, randomly sampled values or quantile values of the observed feature values. The latter two options approximately preserve the marginal distribution of X_A , thus avoiding unrealistic feature values for distributions with outliers.

Each ICE curve reflects the predicted value as a function of the selected set of features in A , conditional on the observed values for all features in $-A$ and a fixed value t . Thus, the ICE algorithm allows for a deeper understanding of the various forms of conditional relationships that are estimated by the black box survival model at different points in time.³⁵

Generally speaking, different shapes of ICE curves at a fixed point in time t , suggest interaction between \mathbf{x}_A and \mathbf{X}_{-A} . Yet, if the ICE curves have different intercepts, i.e. stacked curves, heterogeneity in the model can be difficult to identify. Centering the ICE curves (so-called "c-ICE" curves) to remove level effects at a fixed reference value $X' \sim \mathbb{P}(\mathbf{X}_A)$ simplifies discerning the heterogeneous shapes. The point $(x', \hat{f}(t|x', \mathbf{x}_{-A}^i))$ serves as a reference point for every curve. The g ordered c-ICE curve pairs, for every $i = 1, \dots, n$, for a fixed value of t , are then given by: $\{(x_A^k, \hat{f}_{\text{c-ICE},A}^i(t|x_A^k))\}_{k=1}^g$ with

$$\hat{f}_{\text{c-ICE},A}^i(t|\mathbf{x}_A) = \hat{f}_A^i(t|\mathbf{x}_A) - \hat{f}_A^i(t|x') = \hat{f}(t|\mathbf{x}_A^{\text{grid}}, \mathbf{x}_{-A}^i) - \hat{f}(t|x', \mathbf{x}_{-A}^i). \quad (8)$$

The most common choices for x' are the minimum or maximum values of \mathbf{x}_A . By setting $x' = \min(\mathbf{x}_A)$ all curves originate at 0, thereby eliminating level differences caused by varying \mathbf{x}'_{-A} values. For $x' = \max(\mathbf{x}_A)$ the level of each centered curve reflects the cumulative effect of \mathbf{x}_A on $\hat{f}(\cdot)$ relative to the reference point x' . In this way, the isolation of the combined effect of \mathbf{x}_A on $\hat{f}(\cdot)$ is improved, holding the values of all other features $-A$ fixed.

Different ICE curves are obtained for different values of t . To assess how feature effects differ over time, multiple sets of n ICE curves at different timepoints of interest can be compared. Which timepoints are of particular interest depends on the specific purpose of the analysis, in many cases an equidistant grid of few representative values within the range of $[t_0, \dots, t_m]$ may suffice. It is further possible to reduce the dimensionality to match classic (non-survival) ICE curves by marginalizing over time; we refer to this as ICE-T curves. In the simplest form we can average over the set $T^s = \{t_0, \dots, t_m\}$, such that for the ICE-T curves a set of g ordered pairs is obtained for every $i = 1, \dots, n$: $\left\{ (x_A^k, \frac{1}{|T^s|} \sum_{s=0}^m \hat{f}_A^i(t_s | x_A^k)) \right\}_{k=1}^g$. In case $f(\cdot) = f^S(\cdot)$, the ICE-T value at every point x_A^k are an estimator for the expected probability of survival for a specific instance i at any given timepoint t_s , estimated by the average probability of survival of individual i , if the average is taken over all observed survival times t_{n0}, \dots, t_n . Note that in survival analysis, when referring to the average survival probability, it is commonly referred to the average probability of survival across observations. Alternatively, to obtain a more established identifier, we can simply sum over the observed survival times t_{n0}, \dots, t_n , such that the ordered pairs $\left\{ (x_A^k, \sum_{s=n0}^n \hat{f}_A^i(t_s | x_A^k)) \right\}_{k=1}^g$ estimate the expected survival time for an individual $i = 1, \dots, n$ corresponding to every feature value x_A^k . Practical examples of c-ICE curves on real data can be found in the tutorial Section 3.

ICE curves offer an intuitive and transparent way of assessing the consistency and robustness of model predictions across different observations, aiding in the detection of potential biases or inconsistencies in the model's behavior. They further play a central role in uncovering heterogeneous relationships between features and predictions on an individual-level, drawing attention to both feature-level and feature-time-level interactions in the case of survival outcomes. The known limitations of ICE plots in the classic machine learning setting also carry over to the survival setting ICE plots. ICE plots become increasingly complex and challenging to interpret with a growing number of dimensions, both in terms of the number of features, and in terms of the output, which can be particularly challenging in the survival setting, due to the additional time dimension requirement. Furthermore they are unable to capture high-order interactions and global effects.

2.1.2 | Counterfactual Explanations (CE)

A counterfactual $\mathbf{c}^i = (c_1^i, \dots, c_p^i)^\top$ or "what-if" explanation, identifies the minimum change required in the original feature values $\mathbf{x}^i = (x_1^i, \dots, x_p^i)^\top$ of a particular instance i , such that the model's prediction is modified to align with a predefined outcome.²² Kovalev et al.²⁵ propose a method for counterfactual explanations of machine learning survival models, which is derived from the method introduced by Wachter et al.³⁶. They define an optimization problem to be solved for finding counterfactual \mathbf{c} by minimizing the sum of a loss function $L^{\text{dist}}(\cdot)$ and the Euclidean distance between the original observation and the counterfactual $\|\mathbf{c} - \mathbf{x}\|_2$:

$$\min_{\mathbf{c} \in \mathbb{R}^p} L(\mathbf{c}) = \min_{\mathbf{c} \in \mathbb{R}^p} \{ L^{\text{dist}}(\mathbb{E}(\mathbf{c}), \mathbb{E}(\mathbf{x})) + C \|\mathbf{c} - \mathbf{x}\|_2 \} . \quad (9)$$

The parameter $C > 0$ determines the regularization strength. For L^{dist} Kovalev et al. consider a hinge-loss of the following form:

$$L^{\text{dist}}(\mathbb{E}(\mathbf{c}), \mathbb{E}(\mathbf{x})) = \max(0, r - (\mathbb{E}(\mathbf{c}) - \mathbb{E}(\mathbf{x}))) , \text{ with} \quad (10)$$

$$\mathbb{E}(\mathbf{x}) = \int_0^\infty f^S(t|\mathbf{x}) dt \text{ and } \mathbb{E}(\mathbf{c}) = \int_0^\infty f^S(t|\mathbf{c}) dt . \quad (11)$$

For some $r \geq 0$, minimizing the hinge loss prompts the identification of counterfactuals \mathbf{c} , which increase the distance in mean times to events for \mathbf{c} and \mathbf{x} up to r . In this context, r requires explicit definition by the modeler, as a smallest distance in mean times to events characterizing distinct groups of instances (e.g., patients). The rationale for configuring the loss function in this manner is to produce counterfactual statements such as the following: “Your treatment was not successful because of a small dose of the medicine (one tablet). If your dose had been three tablets, the mean time of recession would have been increased to a required value”. In general, Equation 9 poses a non-convex optimization problem, which Kovalev et al. propose to solve using the particle swarm optimization algorithm³⁷.

To evaluate the counterfactual explanation proposed by Kovalev et al., we can consider four concrete criteria for a good counterfactual explanation defined by Dandl et al.³⁸ and Molnar²²: (1) the prediction associated with \mathbf{c} is close to the desired outcome, (2) \mathbf{c} is close to \mathbf{x} in the feature space \mathcal{X} , (3) \mathbf{c} differs from \mathbf{x} only in a few features, (4) \mathbf{c} is a plausible data point according to the probability distribution $\mathbb{P}(\mathcal{X})$, and (5) the underlying algorithm is able to generate multiple diverse counterfactual explanations. The optimization problem in Equation 9 minimizes two terms. The Euclidean distance between counterfactual \mathbf{c} and original input \mathbf{x} acts as a penalty term for deviations of \mathbf{c} from \mathbf{x} , effectively fulfilling criterion (2). Minimizing the hinge loss as delineated in Equation 10 functions to satisfy criterion (1). Kovalev et al. argue that e.g. doctors rarely think in basic concepts of survival analysis. It is commonly known that medical practitioners usually exhibit a preference for scalar metrics, such as mean time to event, when describing, for instance, at-risk cohorts. Nonetheless, it can be posited that representing the counterfactual by a difference in mean time to event holds limited practical significance and even engenders misleading interpretations in real-world applications. This is exemplified by the illustrative interpretation provided by Kovalev et al., which links the reduction in mean recession time to a medicine dose in a causal manner (see prior paragraph). While the method encourages this causal conclusion, its validity is highly questionable. In general, collapsing the survival distribution or hazard function into one number is associated with a significant loss of information. The mean time to event is particularly problematic, due to its inability to account for censoring, cohort dynamics and time-dependent effects. Oftentimes in clinical or biomedical research, specific percentiles (e.g., the 25th or 75th percentile or the median) or other summary measures may be more clinically relevant than the mean. The main argument in favor of the mean time to event definition is computational convenience. Equation 9 simplifies to a convex optimization problem if the Cox regression model is chosen as a prediction model. Both in their simulation studies as well as their real data examples, Kovalev et al. place significant emphasis on substantiating computational accuracy, notably with regard to the particle swarm optimization algorithm. However, they do not engage in a substantive discourse pertaining to the practical utility and interpretability of counterfactual outcomes when applied to real-world data. Criteria (3)-(5) are not at all considered in their survival counterfactual algorithm. Moreover, the optimization problem is unable to account for categorical data. In essence, the counterfactual algorithm proposed by Kovalev et al. serves as a robust foundational framework upon which to develop more advanced algorithms. These advanced algorithms can be carefully calibrated to accommodate the nuances and distinct requisites for counterfactual explanations that hold practical utility across diverse domains of survival analysis. In the future, more meaningful ways of defining groups of instances to differentiate counterfactuals from the original inputs need to be considered, as well as augmentations to the original algorithm by Wachter et al.³⁶, such as the multi-objective algorithm proposed by Dandl et al.³⁸.

2.1.3 | Local Interpretable Model-Agnostic Explanations (LIME)

Kovalev et al.²³ have proposed an extension of the well-known local interpretable model-agnostic explanations (LIME) algorithm called *SurvLIME*. LIME and *SurvLIME* are specific variants of the idea of local surrogate models. These are designed to approximate the behavior of black-box models in a local region of the input space, usually to provide insights into the decision-making process for one individual prediction. The *SurvLIME* explanation algorithm approximates the cumulative hazard function (CHF) generated by the the black-box model using the Cox regression model’s CHF for the same input example \mathbf{x} . This idea is

based on the fact that the Cox regression is considered an interpretable model, as discussed in Section 2.3. In a first step, a point of interest \mathbf{x} is selected around which a set of nearby points \mathbf{x}^k with $k = 1, \dots, g$ is generated. Then the survival machine learning model is used to predict cumulative hazard functions $f^{\text{CHF}}(t|\mathbf{x}^k)$, $\forall k = 1, \dots, g$. In a next step, the optimal coefficients \mathbf{b} are determined such that the average distance between every pair $f^{\text{CHF}}(t|\mathbf{x}^k)$ and $f_{\text{Cox}}^{\text{CHF}}(t|\mathbf{x}^k, \mathbf{b})$ is minimized over all generated points $\mathbf{x}^1, \dots, \mathbf{x}^g$. The mean distance between every CHF pair over all generated points is considered, since survival models produce functional outputs rather than pointwise outputs as in the classical setting. Each CHF distance is further assigned a weight w^k , which is larger for smaller distances between \mathbf{x} and \mathbf{x}^k and vice versa. A considerable simplification of the resulting minimization problem is induced by the independence of $\varphi(\mathbf{x}, \mathbf{b})$ (see Equation 4) from time t , implying that time and covariates can be considered separately. Kovalev et al. show that the resulting optimization problem is unconstrained and convex and of the form

$$\min_{\mathbf{b}} \sum_{k=1}^g w_k \sum_{s=0}^{\tilde{m}} v_{jk}^2 (\ln f^{\text{CHF}}(\tilde{t}_s|\mathbf{x}^k) - \ln f_0^{\text{CHF}}(\tilde{t}_s) - \mathbf{b}^T \mathbf{x}^k)^2 (\tilde{t}_{s+1} - \tilde{t}_s), \quad (12)$$

with v_{jk} defined as straightening weights to adjust for the difference between the distance of the original CHFs and the distance of the logarithms of the CHFs.

$$v_{sk} = \frac{f^{\text{CHF}}(\tilde{t}_s|\mathbf{x}^k)}{\ln(f^{\text{CHF}}(\tilde{t}_s|\mathbf{x}))} \quad (13)$$

The set of unique, ordered observed times to event corresponding to the local points is defined as $\{\tilde{t}_0, \dots, \tilde{t}_{\tilde{m}}\}$, such that $\tilde{t}_0 = \min_{k=1, \dots, g} t_k$ and $\tilde{t}_{\tilde{m}} = \max_{k=1, \dots, g} t_k$. Then the set $\Omega = [0, t_m]$ can be divided into $\tilde{m} + 1$ subsets such that

1. $\Omega = \cup_{s=\tilde{0}, \dots, \tilde{m}} \Omega_s$
2. $\Omega_{\tilde{m}} = [\tilde{t}_{\tilde{m}}, t_m]$, $\Omega_s = [\tilde{t}_s, \tilde{t}_{s+1})$, $\forall s \in \{\tilde{0}, \dots, \tilde{m} - 1\}$
3. $\Omega_s \cap \Omega_k = \emptyset$ for $\forall s \neq k$.

This segmentation allows the simplification of the Euclidean distance between the logarithmized CHFs from Equation 12.

$$D_{2,k} = \|\ln(f^{\text{CHF}}(\tilde{t}|\mathbf{x}^k)) - \ln(f_{\text{Cox}}^{\text{CHF}}(\tilde{t}|\mathbf{x}^k, \mathbf{b}))\|_2^2 \quad (14)$$

$$= \sum_{s=0}^{\tilde{m}} (\ln f^{\text{CHF}}(\tilde{t}_s|\mathbf{x}^k) - \ln f_0^{\text{CHF}}(\tilde{t}_s) - \mathbf{b}^T \mathbf{x}^k)^2 (\tilde{t}_{s+1} - \tilde{t}_s) \quad (15)$$

Algorithm 1 summarizes the computation of SurvLIME.

Kovalev et al. have also developed modifications to *SurvLIME*. *SurvLIME-Inf*³⁹ uses the L_∞ to define the distance between the CHFs. This choice results in a straightforward linear programming problem and *SurvLIME-Inf* is shown to outperform *SurvLIME* with small training sets. Additionally, in Kovalev et al. (2020)⁴⁰ *SurvLIME-KS* is proposed, which uses Kolmogorov-Smirnov bounds to construct sets of predicted CHFs. They are obtained by transforming CHFs into cumulative distributions functions. The optimization problem is then formulated as a maximin problem. The minimum is defined for the average distance between logarithms of CHFs from the black-box survival model and the surrogate Cox regression model. The maximum is taken over logarithms of all CHFs restricted by the obtained KS-bounds. *SurvLIME-KS* promotes robustness to small training sets and outliers.

Furthermore, building up one the ideas of *SurvLIME*, Utkin et al.²⁷ have proposed *UncSurvEx* a method for uncertainty interpretation of black-box survival model predictions. The technique aims to approximate the uncertainty measure of the

Algorithm 1 The algorithm for computing vector \mathbf{b} for point \mathbf{x}

Require: Training set D ; point of interest \mathbf{x} ; the number of generated points g ; the black-box survival model for explaining $f(\cdot)$

Ensure: Vector \mathbf{b} of important features

- 1: Compute the baseline cumulative hazard function $f_0^{\text{CHF}}(t)$ of the approximating Cox model on dataset D by using the Nelson–Aalen estimator
 - 2: Generate $g - 1$ random nearest points \mathbf{x}^k for every $k = 1, \dots, g$, in a local area around \mathbf{x} , point \mathbf{x} is the g -th point
 - 3: Get the prediction of the cumulative hazard function $f^{\text{CHF}}(t|\mathbf{x}_k)$, for every $k = 1, \dots, g$, by using the black-box survival model
 - 4: Compute weights $w_k = K(\mathbf{x}^*, \mathbf{x}^k)$ of perturbed points, $k = 1, \dots, g$
 - 5: Compute weights $v_{sk} = \frac{f^{\text{CHF}}(\tilde{t}_s|\mathbf{x}^k)}{\ln(f^{\text{CHF}}(\tilde{t}_s|\mathbf{x}^k))}$, $k = 1, \dots, g$, $s = 0, \dots, \tilde{m}$
 - 6: Find vector \mathbf{b} by solving the convex optimization problem in Equation 12
-

black-box prediction by the uncertainty measure of the Cox model prediction.

SurvLIME and its children inherit all limitations from the original LIME method. Like LIME, *SurvLIME* is a purely data-driven, empirical approach that lacks theoretical foundations and guarantees. As a consequence, the quality and stability of the generated explanations is heavily dependent on the selected sample, the chosen perturbation process and the hyperparameters. For instance, in their paper, Kovalev et al. assign weights to every point using the Epanechnikov kernel $w_k = 1 - \sqrt{\frac{\|\mathbf{x} - \mathbf{x}_k\|_2}{r}}$ with $r = 0.5$, providing no further justification on the Kernel choice or comparisons to results using different Kernel functions. Lastly, the explanations obtained from *SurvLIME* are heavily dependent on the chosen surrogate model suffering from its innate restrictions. Employing the Cox regression as a surrogate, implies assuming a local linear relationship between the logarithm of the hazard and the predictors. Furthermore, as discussed in Section 2.3, the proportional hazards and time-independence are assumed to hold locally, which are often not met in real-world datasets. The simulation studies and experiments on real data performed by Kovalev et al. provide little substantiation of the validity of the local explanations provided by the Cox model. The focus of the simulation studies relies on proving the similarity of the true underlying \mathbf{b} coefficients and the coefficients of the approximating Cox model, when assuming the data generating process to follow a Cox model. This emphasis primarily underscores the efficacy of the convex programming algorithm employed, with a lesser focus on evaluating *SurvLIME*'s efficacy as an interpretability method. Notably, the simulation studies exclusively pertain to data conforming to an underlying Cox model. Additionally, the analysis refrains from presenting further comparative assessments between the outcomes of *SurvLIME* and alternative local interpretability methodologies. While certain limitations, such as the examination of varying hyperparameter selections or the formulation of an extension to accommodate time-dependent explanations, may be addressed, it is important to note that *SurvLIME* is bound by the fundamental constraints inherent in the original LIME explanation methodology.

To alleviate some of the drawbacks of *SurvLIME*, Utkin et al. have proposed *SurvNAM*²⁶. The basic idea behind the explanation algorithm *SurvNAM* is to approximate the black-box model by a generalized additive Cox model, in which $\varphi(\mathbf{x}, \mathbf{b})$ is replaced with

$$\varphi(\mathbf{x}, g) = g_1(\mathbf{x}_1) + \dots + g_p(\mathbf{x}_p). \quad (16)$$

The CoxGAM (Cox generalized additive model) is in turn approximated in the form of a neural additive model (NAM), used to learn the shape functions $g_j(\mathbf{x}_j)$, $\forall j \in \{1, \dots, p\}$. One shape function corresponds to one network. These subnetworks may exhibit different architectures, but are trained jointly using backpropagation and have the capacity to learn arbitrarily complex shape functions. To generate local explanations, again synthetic points are randomly generated around an instance of interest \mathbf{x} , for which black-box predictions of the CHF are produced by the model to be explained. To train the neural network, the weighted

Euclidean distance between the CHF of the black box model $f^{\text{CHF}}(t|\mathbf{x})$ and the CHF of the approximating NAM $f_{\text{NAM}}^{\text{CHF}}(t|\mathbf{x}, g)$ is minimized for all generated points. The resulting expected loss function is convex. In contrast to *(Surv)LIME*, the authors specifically encourage the use of *SurvNAM* as a global surrogate model, by simply replacing the synthetic points generated around a local example of interest with the whole training set D . Due to the additive nature of the model, the marginal effect of each feature is independent of the rest, hence the shape functions correspond to feature contribution functions, which can be visualized for explainability purposes. Overall, *SurvNAM* surpasses *SurvLIME* in terms of flexibility and the richness of its output, while also harboring potential for future advancements. The authors have, for example, already included two useful extensions. The first employs the Lasso-based regularization for the shape functions from GAM to produce a sparse representation, which prevents the neural network from overfitting. The second modification adds a linear component to each shape function with some additional weights to be trained, mitigating the vanishing gradient problem. The authors consider the GAM extension of the Cox model sufficiently flexible to adequately capture the black-box model results. This assumption of comparable complexity to the black box model heavily depends on the specific black box model and data analyzed and has so far not been proven in many practical applications. It would, in fact, warrant the question, as to why the interpretable model should not entirely replace the black box model, which is a general flaw inherent in the idea of global surrogate models. The absence of robust guarantees regarding their fidelity to the original model's behavior and the risk of introducing bias due to assuming an additive model structure strike as additional limitations of the *SurvNAM* concept.

2.1.4 | Shapley Additive Explanations (SHAP)

The application of the popular SHAP algorithm⁴¹ to the survival analysis context has been explored by Alabdallah et al.²⁴, Krzyżiński et al.²¹ and Ter-Minassian et al.⁴², who propose distinct approaches for its implementation. SHAP computes the Shapley values⁴³ of the features, which quantify the contribution of each feature to the difference between the model prediction for a given sample and the average prediction of the model. Global explanations can be conveniently derived by aggregating Shapley values across a multitude of instances⁴⁴.

Alabdallah et al. propose *SurvSHAP*, an algorithm enabling the derivation of those global explanations based on the original SHAP algorithm, without directly modifying it for survival analysis. Instead, SHAP is used to explain a proxy classification model that learns the mapping from the input space $\mathcal{X} \in \mathbb{R}^{N \times P}$ to a set of survival patterns $C \in \mathbb{R}^N$. These survival patterns are homogeneous sub-populations with similar survival behavior according to the machine learning survival model's predictions. To achieve this, principal components analysis is employed to reduce the dimensionality of the survival curves to a lower-dimensional representation, denoted as $\mathcal{D} \in \mathbb{R}^{n \times d}$. Subsequently, the curves in the \mathcal{D} space undergo an iterative clustering process, and the resulting sub-populations are compared using log-rank tests. The fraction of significantly different groups is calculated from the total number of comparisons. Finally, the largest number of sub-populations that maximizes the percentage of distinct patterns is selected to cluster the curves in the \mathcal{D} space, resulting in the final set of C clusters. In their experimental evaluation involving both real and synthetic data, Alabdallah et al. propose K-means and a random forest classifier as a default clustering and proxy classification method, respectively. Additionally, they utilize TreeSHAP⁴⁴ as a default base explainer, albeit without performing a sensitivity analyses for these choices. Despite being termed *SurvSHAP*, the algorithm allows for generalization as a methodology rendering any global model-agnostic (or model-specific in the case of the proxy classifier) explanation technique applicable to explain survival patterns of homogeneous sub-populations. Comparable levels of explanatory efficacy can be attained with simple feature importance algorithms, as the unique capabilities of SHAP to yield local feature-level attributions grounded on game-theoretical foundations, remains underutilized.

Krzyżiński et al. introduce *SurvSHAP(t)*, which is a direct modification of SHAP designed for generating time-dependent explanations for any functional output of a (machine learning) survival model. *SurvSHAP(t)* extends the foundational SHAP properties rooted in game theory, including local accuracy, missingness, and consistency, to accommodate the time-dependent

nature of the explanation. Explanations are both computed and evaluated based on the survival function. The algorithm generates the $SurvSHAP(t)$ functions $[\phi_{t_0}(\mathbf{x}^*, j), \dots, \phi_{t_m}(\mathbf{x}^*, j)]$ for every predictor $j \in \{1, \dots, p\}$, pertaining to the observation of interest \mathbf{x}^* across all timepoints $t_s \in t_0, \dots, t_m$. These functions measure the time-dependent feature attributions with regard to the model's prediction. $SurvSHAP(t)$ estimation is implemented by means of the Shapley sampling values algorithm and KernelSHAP. In the Shapley sampling values algorithm the contribution of predictor j in timepoint t_s is calculated as

$$\phi_{t_s}(\mathbf{x}^*, j) = \frac{1}{|\Pi|} \sum_{\pi \in \Pi} e_{t_s, \mathbf{x}^*}^{\text{before}(\pi, j) \cup j} - e_{t_s, \mathbf{x}^*}^{\text{before}(\pi, j)}, \quad (17)$$

where Π is a set of all permutations of feature set $\{1, \dots, p\}$ and $\text{before}(\pi, j)$ denoting a subset of features occurring before j in the ordering $\pi \in \Pi$. The term $e_{t_s, \mathbf{x}^*}^A = \mathbb{E}[\hat{f}^S(t|\mathbf{x}) | \mathbf{x}_A = \mathbf{x}_A^*]$ signifies the expected value corresponding to a conditional distribution with the conditioning applied to some feature set A . More specifically, conditioning is applied to all features from the set A . For KernelSHAP, sample coalitions $z_j \in \{0, 1\}^p$, $j \in \{1, 2, \dots, l\}$ must be defined, such that Z is the matrix of all binary vectors. A value of 1 indicates the presence of the corresponding feature j in a coalition. Additionally, a mapping function $h_x : \{0, 1\}^p \rightarrow \mathbb{R}^p$ is employed to convert binary vectors into the original input space (1 represents the original value). $SurvSHAP(t)$ is estimated as

$$\Phi = (Z^T W Z)^{-1} Z^T W Y, \quad (18)$$

where W is the diagonal matrix containing Shapley kernel weights for each binary vector z :

$$w(z) = \frac{p-1}{\binom{p}{s} f^S(p-s)}, \quad (19)$$

with s the total amount of ones in z . Each row in matrix Y corresponds to the mapping of each row from the Z matrix via the h_x function and thus the survival function values predicted by the underlying machine learning survival model.

The latest addition to the survival SHAP universe is *median-SHAP*, a straightforward adaption of traditional SHAP values to non-inferential survival models. Non-inferential survival models are essentially equivalent to a classic machine learning setting, since a one-dimensional output (usually survival time) is predicted, hence the original SHAP value methodology can be used. Conventional SHAP values are defined in relation to the average prediction, which the authors argue obstructs interpretability in a survival setting, as the average prediction is usually not a plausible instance (see the discussion in Section 2.1.2). Therefore they propose to use the median prediction as a reference value, which by definition is plausible due to aligning with a real instance from the given dataset. Likewise, both summarizing the distribution over model outcomes using expected values (see Equation 17) as well as using the sample means as Monte-Carlo estimators for these expected values is criticized in the survival setting, as both can be problematic in case of a skewed outcome distribution leading to misleading interpretations. Outcome distributions are often right-skewed for survival time predictions models, since there are usually observations experiencing the event after study time. These issues can be mitigated by replacing the mean of the expected change in the model outcome for a coalition from the conventional SHAP value definition with the median. The *median-SHAP* approach is severely limited due to only being applicable to models predicting (median) survival times, which are rarely used in practice. Furthermore, the desirable properties of conventional interventional SHAP values, i.e. local accuracy, missingness, and consistency, no longer hold after the proposed adjustments.

KernelSHAP⁴¹ utilizes a weighted linear regression model to estimate Shapley values. While exact KernelSHAP considers all possible feature subsets and permutations, incurring substantial computational costs, the sampling-based variant of KernelSHAP may compromise accuracy. Computational costs can be reduced when explaining tree-ensemble models like random forests with

the efficient TreeSHAP algorithm⁴⁴. SHAP in general may produce biased or misleading explanations in the presence of feature dependencies due to the extrapolation issue, even when using interventional SHAP values. This issue has been addressed by conditional Shapley values, which often use either Monte Carlo integration or regression to model the conditional expectations⁴⁵. Alternative approaches propose mitigating the extrapolation problem by more thoughtfully generating neighborhood samples, considering the curse of dimensionality⁴⁶, or modeling feature dependencies using variational autoencoders⁴⁷. These avenues present opportunities for further research in the context of survival-focused Shapley values.

2.1.5 | Model-Specific Local Methods

This paper puts its main emphasis on discussing model-agnostic explanation methods. An equally extensive exploration of model-specific techniques is beyond the scope of this paper. In this section, model-specific methods for the two most important machine learning model classes for survival analysis - tree-based models and neural networks - are reviewed briefly.

In the context of survival data, the most pertinent IML techniques for neural networks are feature attribution methods. These methods consolidate various local IML approaches, assigning to each feature the contribution to a specified target variable in the model.¹ One of the first feature attribution methods for neural networks is the (vanilla) gradient method or, especially in the computer vision domain, famously known as saliency maps.⁴⁸ It simply computes the gradients of the chosen prediction with respect to the input features. This computation yields a feature-specific indication of the degree to which a slight alteration in the input variable affects the prediction. The gradient \times input (G \times I) method⁴⁹ was introduced as a straightforward extension to vanilla gradient, in which the gradient is multiplied with the corresponding input value. It takes into consideration the magnitudes of the input features reflecting their relative importance with regard to the prediction, whereas the vanilla gradient treats all features equally in terms of their impact on the model's output. The mathematical motivation behind using the G \times I for feature attribution is a first-order Taylor approximation applied to the prediction. Thereby, it is decomposed into its feature-wise effects by multiplying the gradients with the corresponding input values. In turn, summing these effects over all features, approximately leads to the prediction. An additional extension of the conventional gradient methodology are smoothed gradients (SmoothGrad)⁵⁰. Their primary objective is to mitigate potential fluctuations or abrupt alterations in gradients resulting from various non-linear activation functions. SmoothGrad achieves this by computing gradients from stochastically perturbed input replicas and subsequently averaging them to derive the mean gradient. The rationale behind adding noise in the input is that it helps to smooth out variations in the gradients, providing a more reliable estimate of feature relevance. The layer-wise relevance propagation (LRP) method⁵¹ is a backpropagation-based method to compute layer-wise relevance scores. LRP performs a systematic layer-wise redistribution of upper layer relevance, commencing from the output layer and iteratively progressing until the input layer is reached. This process relies on the weights and intermediate values of the network. The summation of all LRP relevances approximately mirrors the model's prediction, resembling G \times I. There are different rules to distribute the upper-layer relevances to the preceding layers, such as the simple rule, the $\alpha - \beta$ -rule or the ϵ -rule. DeepLIFT⁴⁹ (deep learning important features) is another backpropagation-based approach. It represents the contribution of each feature to the difference in a target neuron's activation between the actual input and the reference input. The target neuron is usually chosen as the output neuron corresponding to the prediction to be explained. The reference input typically represents a baseline or neutral state. It could be an all-zero input or an input chosen based on domain knowledge. As with LRP, the contribution scores are distributed to individual input neurons using specific rules (e.g. path-specific, rescale or linear rules) in a backward propagation process. DeepLIFT offers the flexibility to separately account for the impacts of positive and negative contributions within nonlinearities.

Cho et al.⁵² have successfully employed DeepLIFT for a meta-learning algorithm with Cox hazard loss for multi-omics cancer survival analysis, discovering correlations between DeepLIFT feature importance scores and gene co-enrichment. The integrated

¹Note, that this definition is not limited to neural network specific-methods, SHAP, Shapley values or LIME are also considered feature attribution methods.

gradients method⁵³ combines the desirable properties of gradient based methods (sensitivity²) with those of backpropagation based methods (implementation invariance³). They are defined as the path integral of the gradients along a straightline path from some baseline (usually chosen such that the network prediction is close to zero) to a selected input. Beyond feature attribution methods, there are other techniques for extracting insights from neural network models. Perturbation-based approaches discern prediction-sensitive regions within input images by rendering individual or small pixel regions uninformative, e.g. by masking, altering, or conditional sampling followed by the quantification of resultant changes in prediction probabilities. Moreover, there are both feature attribution and perturbation-based methods that work only on convolutional neural networks, which are primarily tailored for image analysis, for instance gradient-weighted class activation maps (Grad-CAMs)⁵⁴, meaningful perturbation⁵⁵ or guided backpropagation⁵⁶. In addition, neural network specific methods for Shapley value computation have been developed, such as expected gradients⁵⁷, a SHAP-based version of integrated gradients, or DeepSHAP⁴¹, which uses the per node attribution rules from DeepLIFT to approximate Shapley values. Notably, with the exception of DeepLIFT, to the best of our knowledge, none of these techniques has hitherto demonstrated successful application in survival neural networks. The most relevant local method for tree interpretability is a model-specific version of KernelSHAP, on which *SurvSHAP*(t) is based, as discussed in Section 2.1.4. TreeSHAP is a variant of the Shapley values algorithm, specifically designed for the computation of feature attributions in tree-based models⁴⁴. The extension to survival outcomes is a direction for future work.

2.2 | Global Methods

2.2.1 | Partial Dependence Plots (PDPs)

The partial dependence function quantifies the average changes in prediction induced by feature changes.⁵⁸ In this section, we present a formal adaption of the partial dependence concept to survival analysis. For a subset of features $A \subset \{1, \dots, p\}$ (again for notational simplicity we assume $|A| = 1$) and for prediction function $f(\cdot)$ it is defined as

$$f_{\text{PDP},A}(t|\mathbf{x}_A) = \mathbb{E}_{X_{-A}}[f(t|\mathbf{x}_A, X_{-A})] = \int_{-\infty}^{\infty} f^S(t|\mathbf{x}_A, X_{-A}) d\mathbb{P}(X_{-A}). \quad (20)$$

It computes the average outcome for a fixed subset of features (A) with the remaining features ($-A$) varying over their marginal distribution ($d\mathbb{P}(X_{-A})$). Thereby, the partial dependence function quantifies the relationship between the feature set of interest A and the outcome at time t .

In practice, both the true outcome and the marginal distribution $d\mathbb{P}(X_{-A})$ are unknown. The integral over X_{-A} can be estimated by averaging over the n observed training data values for a fixed value of t . If $\{\mathbf{x}_{-A}^1, \dots, \mathbf{x}_{-A}^n\}$ represent the different values of X_{-A} observed in the training data, then for a fixed value of t , Equation 20 can be estimated as

$$\hat{f}_{\text{PDP},A}(t|\mathbf{x}_A) = \frac{1}{n} \sum_{i=1}^n \hat{f}(t|\mathbf{x}_A^{\text{grid}}, \mathbf{x}_{-A}^i). \quad (21)$$

To obtain a partial dependence plot, a set of g ordered pairs, $\{(x_A^k, \hat{f}_{\text{PDP},A}(t|x_A^k))\}_{k=1}^g$, needs to be computed for a fixed value of t . The resulting partial dependence plot, reflects the average prediction over the n observations for fixed t as a function of a feature of interest. Therefore, it is simply the aggregation of the ICE curves over the n observations at every grid point for a fixed point in time. Ideally, ICE and PDP plots at a specified timepoint should be plotted together to avoid obfuscation of heterogeneous effects and interactions.

²Sensitivity: Non-zero attribution to feature, if two inputs differ only in that feature but produce different predictions.

³Implementation invariance: Attributions of two functionally equivalent networks should be equivalent. Two networks are functionally equivalent if their outputs are equal for equal inputs regardless of implementation specifics.

As for the ICE curves, standard PDPs use one feature of interest x_A . The grid value definition follows the same rationale as for the ICE plots. Centered PDP plots, i.e. c-PDPs, are obtained by aggregating the c-ICE curves over the n observations:

$$\hat{f}_{c\text{-PDP},A}(t|\mathbf{x}_A) = \frac{1}{n} \sum_{i=1}^n \left[\hat{f}(t|\mathbf{x}_A^{\text{grid}}, \mathbf{x}_{-A}^i) - \hat{f}(t|x', \mathbf{x}_{-A}^i) \right]. \quad (22)$$

Different PDPs are obtained for different values of t . To assess how global feature effects differ over time, multiple sets of PDPs at different timepoints of interest can be compared. Which timepoints are of particular interest depends on the specific purpose of the analysis. When ICE curves and PDPs are displayed together, an equidistant grid of few representative values within the range of the set $\{t_0, \dots, t_m\}$ may suffice. It is further possible to reduce the dimensionality to match classic PDPs and ICE-T curves by marginalizing over time, analogously we refer to these as PDP-T curves. In the simplest form we can average over $t_s = t_0, \dots, t_m$:

$$\hat{f}_{\text{PDP-T},A}(\mathbf{x}_A) = \frac{1}{|T^s|} \sum_{s=0}^m \frac{1}{n} \sum_{i=1}^n \hat{f}(t_s|\mathbf{x}_A^{\text{grid}}, \mathbf{x}_{-A}^i). \quad (23)$$

In case $f(\cdot) = f^S(\cdot)$, the PDP-T value at every point x_A^k is an estimator for the expected probability of survival across all individuals at any given timepoint, estimated by the average probability of survival across all observations $i = 1, \dots, n$, taken across all observed survival times $t_s = t_{n0}, \dots, t_n$. Note that in survival analysis, the average survival probability commonly refers to the average probability of survival across observations, which is considered as the global feature effect in the PDPs without marginalization. When merely summing over the observed survival times, the generated point pairs estimate the average expected survival time over all instances $i = 1, \dots, n$ corresponding to every feature value x_A^k .

In combination with ICE plots, PDP's offer an intuitive and easily interpretable unification of both local and global feature effects. This facilitates insights into the direction and magnitude of the effects of features on the predicted survival outcome, allows for the detection of complex patterns and interactions and helps evaluating the reliability of the model and detecting potential biases or overfitting. The primary constraint inherent in PDPs, which extends to the survival analysis context, is the so-called extrapolation issue. It arises as a consequence of the underlying assumption of feature independence. In the presence of correlated features, the process of averaging over the marginal distribution of the feature set $-A$, may take unrealistic data points, outside the margins of the observed values into consideration for the computation of the partial dependence profile. Such extrapolation, in turn, leads to unreliable feature effect estimates. This concern is not limited solely to regions beyond the boundaries of observed values; it also pertains to areas with a significant separation between neighboring x_A values, potentially resulting in an inappropriate and volatile relationship with the target variable, particularly in the presence of outliers.³⁵ A notable challenge amplified by the survival analysis setting is the dimensionality limitation. Compared to traditional one-dimensional output settings, the inclusion of time as an additional dimension further complicates the visualization of PDPs, which is by nature limited to three dimensions, obstructing the effective display of feature effects and interactions of multiple features with time.

2.2.2 | Accumulated Local Effects (ALE) Plots

PDPs implicitly assume the independence of the feature of interest of all other features for quantifying and visualizing its main effect on the target. If correlated features are present, the marginal effects shown in the PDP may not accurately reflect the true relationship between target and feature of interest. This is because, in this case, the integral over the marginal distribution of X_{-A} estimated in Equation 20 requires reliable extrapolation beyond the scope of the training data, which cannot be guaranteed by nature of most supervised machine learning models. Marginal plots (M-plots) substitute the marginal density with the conditional

density to avoid such extrapolation:

$$f_{M,A}(t|\mathbf{x}_A) = \mathbb{E}_{X_{-A}}[f(t|X_A, X_{-A})|X_A = \mathbf{x}_A] = \int_{-\infty}^{\infty} f(t|\mathbf{x}_A, X_{-A}) d\mathbb{P}(X_{-A}|X_A = \mathbf{x}_A), \quad (24)$$

where $f_{M,A}(t|\mathbf{x}_A)$ can be crudely estimated as

$$\hat{f}_{M,A}(t|\mathbf{x}_A) = \frac{1}{n(\mathbf{x}_A)} \sum_{i \in N(\mathbf{x}_A)} \hat{f}(t|\mathbf{x}_A, \mathbf{x}_{-A}^i). \quad (25)$$

For some fixed t and $N(\mathbf{x}_A) \subset \{1, \dots, n\}$, the subset of instances for which x_A^i falls into some small neighborhood of \mathbf{x}_A and $n(\mathbf{x}_A)$ are the number of observations in that neighborhood. While M-plots solve the extrapolation issue, conditioning on \mathbf{x}_A introduces the so-called omitted variable bias, if there are at least two correlated features which both are associated with the target. In this case, $\hat{f}_{M,A}(t|\mathbf{x}_A)$ estimates the combined effect of the correlated features on the target.

Accumulated local effects plots (ALE) extend M-plots to obtain an unbiased estimate for the main effects of a feature of interest. The basic idea consists of three parts. The first part constitutes removing unwanted effects of other features by first taking partial derivatives (local effects) of the prediction function with regard to the feature of interest. Then the local effects are averaged over the conditional distribution similar to M-plots to avoid the extrapolation issue. Finally, the averaged local effects are integrated (accumulated) with regard to the same feature of interest to estimate its global main effect, obviating the omitted variable bias. This section constitutes the first formal demonstration of M-plots and ALE plots in the context of survival analysis.

Let the support of \mathbf{x}_A be the interval $S_A = [\min(\mathbf{x}_A), \max(\mathbf{x}_A)]$. For each $k = 0, 1, \dots, g$ let $\mathcal{P}_A \equiv \{z_A^k : k = 0, 1, \dots, g\}$ be a partition of S_A into g intervals with $q_A^0 = \min(\mathbf{x}_A)$ and $q_A^g = \max(\mathbf{x}_A)$. For any $x^* \in S_A$, define $k_A(x^*)$ to be the index of the interval of \mathcal{P}_A into which x^* falls, i.e. $x^* \in (q_A^{k-1}, q_A^k]$ for $k = k_A(x^*)$. Assuming $f(\cdot)$ is differentiable, the uncentered first order ALE main effect for a fixed t is defined as

$$\tilde{f}_{ALE,A}(t|x^*) = \int_{q_A^0}^{x^*} \mathbb{E}_{X_{-A}|X_A=\mathbf{x}_A} \left(\frac{\partial \hat{f}(t|X_A, X_{-A})}{\partial X_A} \Big| X_A = \mathbf{q}_A \right) d\mathbf{q}_A. \quad (26)$$

Usually the centered ALE is considered, which has a zero mean regarding the marginal distribution of the feature of interest:

$$f_{ALE,A}(t|x^*) = \tilde{f}_{ALE,A}(t|x^*) - \int_{-\infty}^{\infty} \tilde{f}_{ALE,A}(t|x^*) d\mathbb{P}(X_A). \quad (27)$$

To estimate the first order ALE effects, a sufficiently fine fixed partition $\{N_A(k) = (q_A^{k-1}, q_A^k] : k = 0, 1, \dots, g\}$ of the sample range of the support S_A is chosen. Customarily, the quantile distribution of X_A is used to create g intervals, with $g - 1$ quantiles as interval bounds $q_A^0, \dots, q_A^{g-1}, q_A^g$. The lower bound q_A^0 is set just below the minimum observation $\min(\mathbf{x}_A)$, and q_A^g is set as the maximum observation $\max(\mathbf{x}_A)$. The local effect of \mathbf{x}_A within each interval is estimated by averaging all observation-wise finite differences. For some $\mathbf{x}^i = (x_A^i, \mathbf{x}_{-A}^i)$, for which $x_A^i \in (q_A^{k-1}, q_A^k]$ the finite difference is computed as $\hat{f}(t|q_A^k, \mathbf{x}_{-A}^i) - \hat{f}(t|q_A^{k-1}, \mathbf{x}_{-A}^i)$. In this way, the conditional expectations (inner integrals over the local effects) are approximated using sample averages across $\{\mathbf{x}_{-A}^i : i = 1, \dots, n\}$ conditional on x_A^i falling into the corresponding interval of the partition. To estimate the outer integral, the local effects are accumulated up to the point of interest x^* .

Let $n_j^i(k)$ be the number of training observations located in interval $N_j^i(k)$, such that $\sum_{k=1}^g n_j^i(k) = n$. Then the formula to

estimate the uncentered first order ALE at point x^* for some fixed t is denoted as

$$\hat{f}_{\text{ALE},A}(t|x^*) = \sum_{k=1}^{k_A(x^*)} \frac{1}{n_A^i(k)} \sum_{i: x_A^i \in N_A^i(k)} [\hat{f}(q_A^k, \mathbf{x}_{-A}^i) - \hat{f}(q_A^{k-1}, \mathbf{x}_{-A}^i)] . \quad (28)$$

Analogously to Equation 27, the centered first order ALE effect for a fixed t is obtained by subtracting an estimate of the average uncentered first order ALE

$$\hat{f}_{\text{ALE},A}(t|x^*) = \hat{f}_{\text{ALE},A}(t|x^*) - \frac{1}{n} \sum_{i=1}^n \hat{f}_{\text{ALE},A}(t|x_A^i) . \quad (29)$$

To assess the interaction of the main feature effects with time, different ALE plots can be plotted for a representative set of the observed survival times. Similar to ICE and PDP, ALE plots can be marginalized over time either by averaging or summing over the unique, ordered observed survival times. For instance, the uncentered first order ALE-T effect would then be estimated as follows

$$\hat{f}_{\text{ALE-T},A}(t|x^*) = \sum_{k=1}^{k_A(x^*)} \frac{1}{n_A^i(k)} \sum_{i: x_A^i \in N_A^i(k)} \left[\frac{1}{|T^S|} \sum_{s=0}^m \hat{f}(t_s | q_A^k, \mathbf{x}_{-A}^i) - \hat{f}(t_s | q_A^{k-1}, \mathbf{x}_{-A}^i) \right] . \quad (30)$$

Essentially, PDP and ALE offer two different methods of quantifying the main effect of a feature of interest at a certain value. Using a set of grid values, the corresponding ALE values $\hat{f}_{\text{ALE},A}(t|x_A^{\text{grid}})$ can be plotted just like the PDP. The values $\hat{f}_{\text{ALE},A}(t|x_A^{\text{grid}})$ are estimates of the change in the prediction, when the feature of interest take the values x_A^{grid} compared to the average predicted survival probability at some timepoint t . For interpreting the ALE-T curves in case $f(\cdot) = f^S(\cdot)$, the difference between average predicted probability of survival until time t_m and over all observations n needs to be kept in mind. When averaging over time, the ALE values are interpreted as the change in average predicted survival probability over time, compared to the average predicted survival probability over time and over observations. Correspondingly, when summing over time, the ALE values represent the change in average predicted survival time with respect to the average predicted survival time.

Since ALE plots accumulate effects in a certain direction, the feature values of the feature of interest need to have a natural order. This is the case for numerical features and ordinal categorical features, but not all categorical features in general. The most commonly used method of instilling an order to categorical features is ranking them according to their similarity based on the remaining features.⁵⁹ Typically, the feature-wise distances are computed using the Kolmogorov-Smirnov distance (for numerical features) or relative frequency tables (for categorical features). After obtaining distances between all categories, multi-dimensional scaling is used reduce the distance matrix to a one-dimensional distance measure based on which the order of the categories is determined.²²

Although ALE plots effectively circumvent the issue of extrapolation and the resultant potential for unreliable feature effect estimates, their interpretation in the presence of correlated features is not straightforward. Under such conditions, extrapolating the feature effect interpretation across computational intervals is not permissible, as ALE feature effects are computed locally, each relying on distinct observations within their designated interval. The accumulation of the local, within-interval feature effects to a smooth curve enhances visual clarity and facilitates interpretation in scenarios with minimal or absent feature correlations, but it can inadvertently lead to misinterpretation when confronted with substantial feature interdependencies. Generally speaking, the main disadvantage of ALE plots is their enhanced conceptual complexity compared to PDPs. Practice has shown that even for stakeholders possessing strong mathematical background knowledge, grasping ALE plots can be challenging.

2.2.3 | Feature Interaction

Feature interaction refers to the collaborative effect of two or more features on the prediction after removing their individual main effects. A common way to estimate interaction strength are Friedman's H-statistics. In this section we focus on two-way interactions measures and a total interaction measure, which we formally adapt to survival analysis. These two measures are of primary interest in most applications, yet the H-statistic can be generalized to any type of interaction. The two-way interaction H-statistics measures the interaction strength between two features a and b for some fixed time point t :

$$H_{ab}^2(t) = \frac{\sum_{i=1}^n [\hat{f}_{\text{PDP},\{a,b\}}(t|x_a^i, x_b^i) - \hat{f}_{\text{PDP},a}(t|x_a^i) - \hat{f}_{\text{PDP},b}(t|x_b^i)]^2}{\sum_{i=1}^n \hat{f}_{\text{PDP},\{a,b\}}^2(t|x_a^i, x_b^i)}. \quad (31)$$

This is simply an estimator for the amount of the variance of the output of the partial dependence explained by the two-way interaction. If \mathbf{x}_a and \mathbf{x}_b do not interact, $H_{ab}^2(t)$ is zero, since the two-way partial dependence function can be decomposed as $\hat{f}_{\text{PDP},\{a,b\}}(t|x_a^i, x_b^i) = \hat{f}_{\text{PDP},a}(t|x_a^i) + \hat{f}_{\text{PDP},b}(t|x_b^i)$. If the interaction statistic is one, the individual partial dependence functions are constant $\hat{f}_{\text{PDP},a}(t|x_a^i) = \hat{f}_{\text{PDP},b}(t|x_b^i)$, meaning only the interaction affects the predicted survival probability. Typically, $H_{ab}^2(t) \in [0, 1]$, yet in rare cases the H-statistic can be greater than 1. This occurs if the variance of the two-way interaction exceeds the variance of the two-dimensional partial dependence.

The total interaction H-statistics measures the interaction strength between feature a and all other features in set $-a$ for a fixed t . Let P be the total set of features $\{1, \dots, p\}$

$$H_a^2(t) = \frac{\sum_{i=1}^n [\hat{f}_{\text{PDP},P}(t|\mathbf{x}^i) - \hat{f}_{\text{PDP},a}(t|x_a^i) - \hat{f}_{\text{PDP},-a}(t|\mathbf{x}_{-a}^i)]^2}{\sum_{i=1}^n \hat{f}_{\text{PDP},P}^2(t|\mathbf{x}^i)}. \quad (32)$$

This now is an estimator for the amount of the variance of the output of the entire function explained by the total interaction. Again the numerator makes use of the fact that in case of no interaction between x_a and \mathbf{x}_{-a} : $\hat{f}_{\text{PDP},P}(t|\mathbf{x}^i) = \hat{f}_{\text{PDP},a}(t|x_a^i) + \hat{f}_{\text{PDP},-a}(t|\mathbf{x}_{-a}^i)$.

To evaluate the interaction strength at different timepoints, interaction plots of $|T^S|$ ordered pairs: $\{(t_s, H^2(t_s))\}_{s=0}^m$ can be generated. Generalized measures of interaction over time can be obtained by marginalizing the H-statistics over time, e.g. $H_{ab}^2 = \frac{1}{|T^S|} \sum_{s=0}^m H_{ab}^2(t_s)$ and $H_a^2 = \frac{1}{|T^S|} \sum_{s=0}^m H_a^2(t_s)$. Note, that the H-statistics are merely measures of interaction strength. To learn more about the type and shape of interactions, ICE, PDP and ALE plots with more than one feature of interest can be analyzed. Since the H-statistics are calculated based on partial dependence functions, feature independence is innately assumed. Hence, the H-statistics are unreliable if features correlate strongly and the partial dependence function fails to correctly quantify the main feature effects.

Friedman's H statistic is a versatile and robust tool for assessing interaction effects, offering meaningful insights due to being founded on partial dependence decomposition. Therefore its utility extends beyond identifying solely linear interactions, as it is adept at detecting interactions in various forms. Furthermore, its dimensionless nature facilitates comparisons across features and even different models. The assessment of the H-statistic can entail substantial computational costs, with a maximum of $2n^2|T^S|$ prediction calls for the two-way interaction statistic and up to $3n^2|T^S|$ calls for the total interaction statistic. Therefore, practical implementation often involves the calculation of H-statistics on a random sample of m observations with $m < n$, introducing potential instability in the H-statistic estimate. Additionally, a noteworthy limitation of the H-statistic lies in the lack of a model-agnostic statistical test for determining whether an interaction is significantly greater than zero. The current testing procedure entails the reestimation of the underlying model, excluding the relevant interactions, a practice not always feasible, in particular for complex machine learning models. Furthermore, no guidelines for evaluating the strength of interactions are

established, i.e. at which thresholds an interaction is considered strong, moderate or weak is ambiguous. This is amplified by the lack of a definitive upper bound of the H-statistic, which can exceed a value of 1. This may occur when the variance of the two-way interaction surpasses that of the two-dimensional partial dependence plot. The H-statistic values can be potentially overinterpreted, falsely inferring as a strong interaction effect for spurious interactions, i.e. if the total effect of two features is weak, but predominantly consists of interactions. Moreover, akin to PDPs and ICE plots, accurate H-statistic estimates hinge on the assumption of feature independence. In cases involving highly correlated features, the H-statistic values may become inflated due to the integration of improbable feature combinations.

2.2.4 | Feature Importance

Complementary to feature effects methods, such as ICE, PDP and ALE, so-called feature importance methods aim to quantify the extent of which each feature contributes to the predictive performance of a machine learning model. In this section, the three common feature importance techniques, permutation feature importance (PFI)⁶⁰, Leave-One-Covariate-Out (LOCO)⁶¹ and conditional feature importance (CFI)^{62;63;64;65} are adapted to survival analysis.

Permutation feature importance (PFI)⁶⁶ quantifies the importance of a specific feature of interest j as the change in the model's prediction error induced by permuting \mathbf{x}_j and therefore breaking its association with the target. Small or no changes in the model error imply that the model does not rely heavily on the feature for prediction, thus characterizing a feature of low importance. Important features induce large changes in the model error, since the model does depend strongly on the feature for making predictions. The permutation feature importance algorithm, based on Fisher et al.⁶⁶ and adapted for survival analysis, consists of the steps denoted in Algorithm 2.

Algorithm 2 Permutation Feature Importance

Require: Trained model $\hat{f}(\cdot)$, feature matrix \mathbf{X} , observed survival times vector $\mathbf{t}^{\text{obs}} = [t_{0n}, \dots, t_n]$, loss function $L(\mathbf{t}^{\text{obs}}, \hat{f}(\cdot))$

- 1: Estimate the model loss of the original model $L(\mathbf{t}^{\text{obs}}, \hat{f}(\mathbf{t}^{\text{obs}}|\mathbf{X}))$
 - 2: **for** each feature $j \in \{1, \dots, p\}$ **do**
 - 3: Generate a permuted feature vector $\tilde{\mathbf{x}}_j$ to replace \mathbf{x}_j inducing the permuted feature matrix $\tilde{\mathbf{X}}$
 - 4: Compute the loss based on the predictions of the permuted feature matrix $L(\mathbf{t}^{\text{obs}}, \hat{f}(\mathbf{t}^{\text{obs}}|\tilde{\mathbf{X}}))$
 - 5: Calculate the PFI as a difference $\text{FI}_j^d = L(\mathbf{t}^{\text{obs}}, \hat{f}(\mathbf{t}^{\text{obs}}|\mathbf{X})) - L(\mathbf{t}^{\text{obs}}, \hat{f}(\mathbf{t}^{\text{obs}}|\tilde{\mathbf{X}}))$ or quotient $\text{FI}_j^q = \frac{L(\mathbf{t}^{\text{obs}}, \hat{f}(\mathbf{t}^{\text{obs}}|\mathbf{X}))}{L(\mathbf{t}^{\text{obs}}, \hat{f}(\mathbf{t}^{\text{obs}}|\tilde{\mathbf{X}}))}$
 - 6: **end for**
 - 7: Sort features by descending importance FI_q or FI_d
-

In the permutation step of permutation feature importance, the feature of interest j is replaced with an independent sample from the marginal distribution $\mathbb{P}(X_j)$. Hence, if correlated features are present in the data, potentially unrealistic data points are created, leading to the model extrapolating its predictions outside the range of the original data. The main idea of **conditional feature importance (CFI)** is to resample the feature of interest from the conditional distribution, such that the joint distribution is preserved, i.e. $\mathbb{P}(X_j|X_{-j})\mathbb{P}(X_{-j}) = \mathbb{P}(X_j, X_{-j})$. One concrete implementation of a conditional feature importance measure is the conditional predictive impact (CPI), originally developed by Watson and Wright⁶⁴ and extended to mixed data by Blesch et al.⁶⁵. In CPI, the conditional resampling step is executed by means of knockoff sampling algorithms. The feature of interest j is replaced with a knockoff, retaining the covariance structure of the input features, while being independent of the target, conditional on $-j$, i.e., all other features apart from j . The detailed computation steps are denoted in Algorithm 3. The algorithm is similar to that of PFI, but instead of permuting \mathbf{x}_j , it is replaced by a knockoff copy. The choice of the knockoff sampler depends on the type of input data. Furthermore, the conditional predictive impact method offers the added benefit of an integrated conditional independence test, that can be executed within the framework of paired t-tests or Fisher exact test for small samples.

Algorithm 3 Conditional Predictive Impact

Require: Trained model $\hat{f}(\cdot)$, feature matrix \mathbf{X} , observed survival times vector $\mathbf{t}^{\text{obs}} = [t_{0n}, \dots, t_n]$, loss function $L(\mathbf{t}^{\text{obs}}, \hat{f}(\cdot))$

- 1: Estimate the model loss of the original model $L(\mathbf{t}^{\text{obs}}, \hat{f}(\mathbf{t}^{\text{obs}}|\mathbf{X}))$
- 2: **for** each feature $j \in \{1, \dots, p\}$ **do**
- 3: Generate a knockoff $\tilde{\mathbf{x}}_j$ to replace \mathbf{x}_j inducing the augmented feature matrix $\tilde{\mathbf{X}}$
- 4: Compute the loss based on the predictions of the permuted feature matrix $L(\mathbf{t}^{\text{obs}}, \hat{f}(\mathbf{t}^{\text{obs}}|\tilde{\mathbf{X}}))$
- 5: Calculate the CPI as a difference $\text{FI}_j^d = L(\mathbf{t}^{\text{obs}}, \hat{f}(\mathbf{t}^{\text{obs}}|\mathbf{x})) - L(\mathbf{t}^{\text{obs}}, \hat{f}(\mathbf{t}^{\text{obs}}|\tilde{\mathbf{x}}))$ or quotient $\text{FI}_j^d = \frac{L(\mathbf{t}^{\text{obs}}, \hat{f}(\mathbf{t}^{\text{obs}}|\mathbf{X}))}{L(\mathbf{t}^{\text{obs}}, \hat{f}(\mathbf{t}^{\text{obs}}|\tilde{\mathbf{X}}))}$
- 6: **end for**
- 7: Sort features by descending importance FI_q or FI_d

Leave-one-covariate-out (LOCO)⁶¹ is a technique used to assess the importance of individual features by fitting two separate models, one on the full feature vector \mathbf{X} and one on the feature vector excluding the feature of interest $\mathbf{X}_{-j} = \mathbf{X} \setminus \{\mathbf{x}_{-j}\}$ and comparing their prediction errors. The steps are shown in Algorithm 4.

Algorithm 4 Leave-One-Covariate-Out Importance

Require: Trained model $\hat{f}(\cdot)$, feature matrix \mathbf{X} , observed survival times vector $\mathbf{t}^{\text{obs}} = [t_{0n}, \dots, t_n]$, loss function $L(\mathbf{t}^{\text{obs}}, \hat{f}(\cdot))$

- 1: Estimate the model loss of the original model $L(\mathbf{t}^{\text{obs}}, \hat{f}(\mathbf{t}^{\text{obs}}|\mathbf{X}))$
- 2: **for** each feature $j \in \{1, \dots, p\}$ **do**
- 3: Generate feature matrix \mathbf{X}_{-j} by removing feature j from the original feature matrix \mathbf{X}
- 4: Fit a new model $\hat{f}_{-j}(\mathbf{t}^{\text{obs}}|\mathbf{X}_{-j})$ on the feature matrix \mathbf{X}_{-j}
- 5: Calculate the LOCO FI as a difference $\text{FI}_j^d = L(\mathbf{t}^{\text{obs}}, \hat{f}_{-j}(\mathbf{t}^{\text{obs}}|\mathbf{X}_{-j})) - L(\mathbf{t}^{\text{obs}}, \hat{f}(\mathbf{t}^{\text{obs}}|\mathbf{X}))$ or quotient $\text{FI}_j^q = \frac{L(\mathbf{t}^{\text{obs}}, \hat{f}_{-j}(\mathbf{t}^{\text{obs}}|\mathbf{X}_{-j}))}{L(\mathbf{t}^{\text{obs}}, \hat{f}(\mathbf{t}^{\text{obs}}|\mathbf{X}))}$
- 6: **end for**
- 7: Sort features by descending importance FI_j^d or FI_j^q

For statistical inference, one-sided hypothesis tests of the form:

$$H_0 : \text{FI}_j \leq 0 \text{ versus } H_1 : \text{FI}_j > 0 \quad (33)$$

can be performed for the feature importance values obtained from either of the three methods presented. Originally proposed to mitigate the bias of PFI towards categorical features with many categories, the permutation importance (PIMP) algorithm⁶⁷ provides p-values for the test in Equation 33. The distribution of the PFI values under H_0 is computed by permuting the target to break the association with the features and fitting a distribution to the PFI scores computed under H_0 . Lei et al.⁶¹ rely on the asymptotic normal distribution of the mean-based LOCO FI scores to construct confidence intervals and hypothesis tests corrected for multiple testing for $j \in \{1, \dots, p\}$. To improve stability, they alternatively suggest nonparametric tests based on LOCO FI scores calculated as median decreases in loss, in the form of sign tests or the Wilcoxon signed-rank tests. For CPI scores, Watson and Wright⁶⁴ show that by application of the central limit theorem, one-sided t-tests can be used to evaluate Equation 33 when samples are sufficiently large. For small sample inference, Fisher exact tests are proposed. For further details on inference, refer to the respective papers.

The key to adapting all of the above feature importance measures for survival analysis is the use of appropriate error metrics suitable for survival models. Time-dependent performance measures such as the Brier score, the cumulative/dynamic AUC or

the log-loss can be used to obtain $|T^S|$ ordered pairs: $\{(t_s, FI_j(t_s))\}_{s=0}^m$, such that the feature importance can be visualized over time. Single-value performance measures, such as integrated Brier score, log-loss or AUC as well as the concordance index produce outcomes akin to classic feature importance plots, with one feature being associated with one feature importance value.

2.2.5 | Functional Decomposition

Functional decomposition is a core concept in interpretable machine learning. It refers to the decomposition of complex, high-dimensional machine learning model output functions into more understandable functional components, including feature main effects and lower-level interactions, often for the purpose of visualization. One and two-dimensional components are one and two-dimensional real-valued functions that can be plotted. In this section we delineate how some of the most popular functional decomposition approaches can be adapted to suit survival outcomes.

Let $A \subseteq \{1, \dots, p\}$ be the set of all possible feature combinations. The general decomposition is then denoted as

$$\hat{f}(t|\mathbf{X}) = \sum_{A \subseteq \{1, \dots, p\}} \hat{f}_A(t|\mathbf{X}_A), \quad (34)$$

where a component $\hat{f}_A(t|\mathbf{X}_A)$ only includes the features in A . Note, that the right-hand side of Equation 34 is not identified, i.e., it can be changed without changing the left-hand side. Different constraints can be imposed to uniquely identify and best reflect the contribution of each feature subset to $\hat{f}(t|\mathbf{X})$. In theory, $\hat{f}(t|\mathbf{X})$ can be decomposed into $\sum_{j=1}^p \binom{p}{j} = 2^p$ possible functions. In practice however, we are often only interested in the intercept term ($A = \emptyset$), main effects ($|A| = 1$) and two-way interactions ($|A| = 2$). Different methods exist for obtaining the decomposed functional terms. These include (generalized) functional ANOVA^{68;69}, accumulated local effects⁵⁹, statistical regression models and q -interaction SHAP⁷⁰.

In **functional ANOVA**, each component is defined by

$$\hat{f}_A(t|\mathbf{X}) = \int_{X_{-A}} \left(\hat{f}(t|\mathbf{X}) - \sum_{B \subset A} \hat{f}_B(t|\mathbf{X}) \right) dX_{-A}. \quad (35)$$

To compute a component $\hat{f}_A(t|\mathbf{X})$, the components of all subsets of A ($B \subset A$) are subtracted from the expected value of the prediction function with regard to all features not in set A (X_{-A}), assuming that all features follow a uniform distribution over their respective range of values. By subtracting the lower-order components, their corresponding effects are removed, if a higher-order effect is to be computed, as well as it ensures the estimated effect to be centered. In this way, the computation is iterative, since lower-order components are required for the computation of higher-order components.

Integrating over a uniform distribution when features are dependent, leads to a new dataset that deviates from the joint distribution and predicts improbable feature combinations. This issue of extrapolation, similar to those discussed in previous sections, can cause functional ANOVA results to be biased. To control for the effect of dependence between input features, **generalized functional ANOVA** was introduced by Hooker⁶⁹. In the following, we will show how this method can be adapted to survival outcomes. The uniform distribution of the features on the unit cube used for functional ANOVA, is replaced with a general time-dependent weighting measure $w(t|x)$. The components are jointly defined as projections of the prediction function onto the space of additive functions under the inner product

$$\langle F, G \rangle_w = \int_{\mathbb{R}^p} G(t|\mathbf{X})f(t|\mathbf{X})w(t|\mathbf{X}) . \quad (36)$$

The projection operator may be defined with respect to any \mathcal{L}^2 weight function, provided certain identifiability constraints are

maintained. Explicitly, all the components $\{f_A(t|\mathbf{X}_A) \mid A \subseteq P = \{1, \dots, p\}\}$ are jointly defined as satisfying

$$\hat{f}_A(t|\mathbf{X}_A) = \operatorname{argmin}_{G_A \in \mathcal{L}^2(\mathbb{R}^A)} \int \left(\hat{f}(t|\mathbf{x}) - \sum_{A \subseteq P} G_A(t|\mathbf{X}_A) \right)^2 w(t|\mathbf{X}) d\mathbf{X}, \quad (37)$$

subject to the hierarchical orthogonality conditions, which replaces the orthogonality condition from functional ANOVA with

$$\forall B \subseteq A, \forall G_A : \int \hat{f}_A(t|\mathbf{X}_A) G_B(t|\mathbf{X}_B) w(t|\mathbf{X}) d\mathbf{X} = 0, \quad (38)$$

where zero means and variance decomposition hold as for functional ANOVA. In a general supervised learning context, Hooker shows that Equation 37 subject to Equation 38 produces a unique decomposition given that the support of w is an open set and $f(t|x) : [0, 1]^p \rightarrow \mathbb{R}$.

Accumulated local effects also constitute a functional decomposition method, since it holds that

$$\hat{f}(t|\mathbf{x}) = \sum_{A \subseteq \{1, \dots, p\}} \hat{f}_{A,ALE}(t|\mathbf{x}_A). \quad (39)$$

The components obtained from ALE decomposition satisfy the pseudo-orthogonality property, instead of hierarchical orthogonality as imposed by (generalized) functional ANOVA. Apley and Zhu⁵⁹ argue that pseudo-orthogonality is preferable to hierarchical orthogonality, since it does not mix marginal feature effects. Additionally, ALE has the advantage of allowing for a hierarchical estimation of components, avoiding the computational complexities associated with an estimation of the joint distribution.

The **statistical regression model** approach presents a bottom-up approach for model decomposition, by enforcing simplifying constraints in the modelling process. In its simplest form, regression models, such as the CoxPH model, or generalized additive models (GAMs) with varying degrees of interactions are fitted to the data. Since any likelihood-based regression model, such as the CoxPH model, can be transformed to a GAM, as introduced by Hastie et al.⁷¹, this approach is readily transferable to survival analysis. Hastie and Tibshirani⁷² and Bender et al.⁷³ further provide detailed tutorials on the use of GAMs for time-to-event data.

Hiabu et al.⁷⁰ propose a new identification, equivalent to **q-interaction SHAP**⁷⁴. Theoretically, their results can be applied to any model, including survival machine learning models and they provide an algorithm for calculation of exact q-interaction SHAP for tree-based models. Their identification requires $\hat{f}(t|\mathbf{X})$ to be decomposed as described in Equation 39 such that

$$\sum_{C \cap A \neq \emptyset} \int \hat{f}_C(t|\mathbf{X}_C) \hat{p}_A(\mathbf{X}_A) d\mathbf{X}_A = 0, \quad (40)$$

with \hat{p}_A some estimator of the density p_A of X_A . Given any initial estimator $\hat{f}_A^{(0)} \mid A \subseteq 1, \dots, p$, the unique set of functions $\hat{f}^* = \{\hat{f}_A^* \mid A \subseteq 1, \dots, p\}$ that satisfy Equation 40 are defined by

$$\hat{f}_A^*(t|\mathbf{X}_A) = \sum_{B \subseteq A} (-1)^{|A \setminus B|} \int \hat{f}^{\text{sum}}(t|\mathbf{X}) \hat{p}_{-B}(\mathbf{X}_{-B}) d\mathbf{X}_{-B}, \quad (41)$$

where $\hat{f}^{\text{sum}}(t|\mathbf{X}) := \sum_A \hat{f}_A^{(0)}(t|\mathbf{X}_A) = \sum_A \hat{f}_A^*(t|\mathbf{X}_A)$. The major novelty of this decomposition is that it marries local and global explanations. This is because, on the one hand, (interventional) SHAP values can be extracted from the identification as weighted averages of the components. This allows for a decomposition of simple SHAP values into main effects and all involved interaction effects, extending the concept of functional decomposition to a local explainability scale. On the other hand, global partial dependence plots can be described by the main effect terms plus the intercept. This also holds for higher-order PDPs; in this case all feature sets that contain the feature of interest are included.

The concept of functional decomposition is limited by the dimensionality restriction for higher-order interactions. More specific limitations depend on the specific methodology used. While functional ANOVA suffers from the extrapolation issue in the presence of dependent features, as explained above, in generalized functional ANOVA the components may mix marginal effects of correlated features. This depends on the choice of the weighting function due to the hierarchical orthogonality condition. Furthermore, its estimation process is rather computationally intensive, requiring the solution of a large, weighted linear system. Although possessing computational advantages and potentially more favorable theoretical characteristics in contrast to the (generalized) functional ANOVA as discussed earlier, accumulated local effects fail to offer a variance decomposition. Consequently, there is no assurance that the variance of the functional components aggregates to the total variance of the function, thereby diminishing its interpretability from a statistical perspective. Regression model based decomposition becomes difficult in the presence of feature interactions, since these have to be specified manually. Not properly identifying interactions or the presence of feature correlations may also lead to biased results for main effects due to a failure to comply with underlying assumptions, e.g., in case the CoxPH model is used for decomposition. This is closely linked to the concerns surrounding global surrogate models, discussed in Section 2.1.3. Estimation of functional decomposition based on SHAP values is generally computational intensive. For example, the q -interaction SHAP method described above, can theoretically be applied to any prediction model, but is currently only feasible to compute on tree-based models.

2.2.6 | Model-Specific Global Methods

The feature visualization approach⁷⁵ delves into identifying inputs closely aligned with the training dataset that elicit heightened activation in specific units within a neural network. Therein, “unit” pertains to individual neurons, channels (also referred to as feature maps), or entire layers of the neural network. The foundation of the feature visualization approach is an optimization problem, which can be solved using various optimization and regularization techniques. For example, training images or (combinations of) tabular features that maximize the activation can be selected. Alternatively, new images or feature (combinations) can be generated employing some regularizing constraints. The network dissection approach by Bau et al.⁷⁶ connects highly activated areas of convolutional neural net (CNN) channels with human concepts. It measures the CNN channel activations for training images annotated with human-labeled visual concepts and quantifies the activation-concept alignment with the intersection over union (IoU) score. It is built on the assumption that CNN channels learn disentangled features. The testing with concept activation vectors (TCAV) method goes one step further by training a binary classifier separating the activations generated by a human-labeled concept dataset from those generated by the random dataset. The model’s sensitivity to specific concepts is gauged through the directional derivative of the prediction in the direction of the coefficient vector of the trained binary classifier - the so-called concept activation vector (CAV). A statistical test for the overall conceptual sensitivity of an entire class can be defined using the ratio of inputs with positive conceptual sensitivities to the number of inputs for a class for multiple random datasets. To date, none of the mentioned approaches has been employed within the domain of survival neural networks. Zhong et al.⁷⁷ approach global interpretability for survival neural networks by using a linear surrogate model for a subset of features and then model the rest of the features by an arbitrarily complex neural network. However, it is crucial to note that this methodology does not inherently address the broader challenge of enhancing the interpretability of neural networks. A majority of methods for global neural network interpretability are either predominantly constrained to image data or insufficiently explored for tabular data. In the context of survival data, this is only relevant if images serve as inputs for the survival prediction.

While particularly popular for neural networks, model-specific feature attribution methods likewise exist for tree-based machine learning models. Here, however, the contribution score of individual features is usually understood globally rather than locally, quantifying the effects on the overall predictions made by the ensemble model. One common technique for tree ensemble attribution is feature importance, as many of the popular feature importance measures, such as the permutation feature importance (PFI) or mean decrease of accuracy (MDA) and impurity importance or mean decrease of impurity (MDI) have

originally been developed in the contexts of random forests⁶⁰. Later, they have been extended to work for a large class of models, which is why they are discussed in Section 2.2.4. Another global tree interpretability technique based on the idea of surrogate trees is to simplify a complex ensemble of decision trees to a few or one representative tree. The core idea behind representative tree algorithms typically involves evaluating tree similarity using a distance metric.⁷⁸ Distance measures can encompass various aspects of similarity, e.g. predictions, clustering in terminal nodes, the selection of splitting features, or the level and frequency at which features are chosen in both individual trees and ensembles. The representative tree is typically the one demonstrating the highest mean similarity to all other trees. Alternatively, clustering algorithms can be applied to identify multiple representative trees from distinct clusters.⁷⁹

2.3 | Interpretable Models

2.3.1 | Statistical Survival Models

Intrinsically interpretable survival models allow to extract humanly interpretable insights regarding factors affecting survival probabilities or hazard rates of individual or groups of instances over time. (Semi-)Parametric statistical survival models usually provide interpretable coefficients or parameters. In the parametric Weibull model, for example, the scale parameter represents the rate of event occurrence. Accelerated failure time models⁸⁰, such as the log-normal or the log-logistic model, specify directly how the survival time is affected by covariates. Decision tree-based models are also widely recognized for their high interpretability. This is due to their ability to divide data into segments based on covariate values, resulting in discernible decision rules that make the resulting branches and nodes easily explainable.

The most-frequently used interpretable survival model is certainly the semi-parametric Cox regression model¹ (see Section 1.1). Grounded in its historic and widespread use in clinical and epidemiological research, most survival researchers and practitioners would presumably argue in favor of the Cox model's intrinsic ease of interpretability. Indeed, due to the linearity assumption for $\varphi(\mathbf{x}, \mathbf{b})$, which implies the proportional hazard assumption, the signs and the magnitudes of the coefficients $\mathbf{b}^\top = (b_1, \dots, b_p)$ can be used to quantify the direction and strength of the relationship between feature and prediction. In general, statistically significant coefficient estimates with large absolute values indicate important features. Yet, information on relative feature importance for a given prediction can only be obtained by comparing the absolute values of the coefficients multiplied by the values of its features $|x_j^t \times b_j|$, since the coefficients can be of different scales. A large part of the popularity of the Cox regression model is rooted in the hazard ratio interpretation. The hazard ratio of a feature j can be computed as $\text{HR}_j = \exp(b_j)$, representing the relative change in the hazard rate associated with a one-unit change in feature j . The proportional hazard assumption implies constant hazard ratios over time, further simplifying the interpretation. It must be taken into account however, that the hazard ratio for a distinct feature is a measure conditional on $T \geq t$. This complicates the interpretation even for randomized studies in which the proportional hazard assumption holds, as subjects are no longer comparable for larger t values, if other factors beside the feature of interest influence the time to event. Moreover, in practice the strong assumptions of the Cox regression model are often not met, particularly the assumption of proportional hazards or no time-varying effects of features.² Moreover, the Cox model suffers from the noncollapsibility problem.³ If an unobserved covariate exerts influence on the time-to-event outcome, the marginal model, conditioned solely on the observed covariates, deviates from a Cox regression model. Consequently, this deviation introduces bias in the estimates of crude hazard ratios when compared to adjusted hazard ratios. More recently, Martinussen⁴ has further provided mathematical proof, that hazard ratios can not be interpreted causally unless they are unity (no causal effect) or the unrealistic and untestable assumption of potential outcomes under exposure vs. no exposure being independent of each other is satisfied. These factors show that the Cox's models presumed ease of interpretation is a fallacy of ease of applicability. Additional drawbacks of the Cox regression model include a decline in performance when handling datasets with high dimensions or correlated features. The Cox model further fails to capture complex interactions or

non-linear feature effects if these are not manually specified. In summary, this highlights the need for developing and deploying a broader and universally applicable spectrum of models and explainability methods, suitably tailored to address the challenges posed by censored data. This pertains not solely to the realm of complex machine learning models but extends to encompass classical statistical approaches for the purpose of transcending and augmenting conventional modes of comprehending outputs, such as the hazard ratios.

2.3.2 | Interpretable Machine Learning Survival Models

In general, all survival models that produce some form of output parameters that are linked in some manner to a human-intelligible representation of temporal progression within time-to-event data, can be categorized as interpretable. Discussing them all is beyond the scope of this paper. Given our primary emphasis on the interpretability of machine learning model outputs, we concentrate on particularly salient model categories in this context.

In the field of neural networks and deep learning in recent years interesting interpretable survival models have been developed, which we choose to highlight due to their aim of amalgamating the predictive capabilities of neural networks and deep learning models with outcomes that are amenable to interpretation. A group of deep learning approaches strives to achieve interpretability by adhering closely to the traditional Cox regression model. For instance, in their work, Xie & Yu⁸¹ suggest employing a neural network to fit a mixture cure rate model. This model maintains the proportional hazards structure for uncured subjects. With *WideAndDeep* a wide and deep survival neural network, Pölsterl et al.⁸² combine the output of a neural network analyzing unstructured image data with the output of a Cox regression model handling structured tabular clinical data. Thus, the conventional Cox regression interpretability is retained for the structured features.

An alternative group of deep learning methodologies draws inspiration from the techniques used to induce explainability in other semi-parametric survival models. Within this context, an appealing category of models are additive survival models. Source of their inherent intrinsic interpretability are feature level contribution functions, quantifying the relationship between feature values and prediction functions at different timepoints. They can be readily extracted due to the additive nature of the models and aggregated to overall feature importance scores. These scores are measured as mean individual feature contributions on the survival probability or hazard at pre-specified timepoints. Central additive statistical models are generalized additive models^{71;72;73}, which are discussed further in the context of functional decomposition (Section 2.2.5). Wu & Witten⁸³ additionally introduce an additive Cox proportional hazards model, wherein each additive function is derived by means of trend filtering. Several machine learning models incorporate additive model structures as a means to augment their interpretability. *SURVLSSVM*, an additive survival extension of least-squares support vector machines, was proposed by Van Belle et al.⁸⁴. It uses componentwise kernels, allowing to estimate and visualize feature effects in functional forms. Xu & Guo²⁹ (*CoxNAM*) and Rahman & Purushotham^{28;85} (*PseudoNAM* and *Fair PseudoNAM*) have developed neural additive models (NAMs) for survival outcomes based on the idea of Agrawal et al.⁸⁶. They combine some of the expressivity of deep neural networks, particularly their ability to capture non-linearity with the inherent interpretability of generalized additive models. In similar vein, in *DeepPAMM*, Kopper et al.⁸⁷ embed piecewise exponential additive mixed models (PAMMs)⁷³ into a highly flexible neural network, which can accommodate multimodal data, time-varying effects and features, the inclusion of mixed effects to model repeated or correlated data, as well as different survival tasks. The predictor modelled by *DeepPAMM* contains a structured additive part corresponding to a PAMM model representation and an unstructured part, capturing high-dimensional interactions between the features from the structured part using a customizable neural network. The structured part estimates inherently interpretable feature effects, providing classical statistical interpretability, e.g. through feature effect plots.

Furthermore, many deep learning models explore dimensions of interpretability that extend beyond the ideas of existing semi-parametric methods. Chen⁸⁸ proposes *survival kernel*, a deep kernel survival model, in which a kernel function is learned, which is used to predict the survival probability for unseen observations based on the most similar training observations. More

specifically, kernel netting⁸⁹ is used to induce interpretability, by partitioning the training data into clusters and then representing unseen instances as a weighted combinations of a few clusters. The clusters can be interpreted classically by comparing the Kaplan-Meier survival curves across clusters. Alternatively, a heatmap visualization of the fraction of points in a cluster with specific feature values can be employed to deduct feature-based characteristics for each cluster. Since kernel weights determine the contribution of each cluster to a new data instance, local interpretations of the relative importance of different clusters for the hazard function prediction can be extracted.

In the domain of multi-omics data analysis, a cluster of applications has emerged, wherein interpretability is achieved through the attribution of biological significance to nodes. In these methodologies, the pursuit of interpretability is a fundamental design objective. Consequentially, significant attention is directed towards assessing the interpretable outcomes in a comprehensible, comprehensive, sensitive and diverse manner. Hao et al.³¹ developed a pathway-based sparse deep survival neural network, named *Cox-PASNet*. Its architecture is key to the intrinsic interpretability. A pathway layer incorporates prior knowledge on pathways characterizing biological processes, with the values indicating the active/inactive status of a single pathway in a biological system. Hidden/integrative layers show the interactive (nonlinear and hierarchical) effects of multiple biological pathways. The observations are separated into risk groups by prognostic index outcome of the tuned network. For the risk groups layer-wise feature importance scores are assigned comparing the average absolute partial derivatives, visualized by heatmaps. A log-rank test and the comparison of Kaplan-Meier survival curves allows the classification of top-ranked features as prognostic factors. Additionally, important pathway and integrative nodes are visualized by t-SNE, to illustrate hierarchical and nonlinear combinations of pathways. Hao et al.³⁰ extend these intrinsic means of interpretation to a biologically interpretable, integrative deep learning model that integrates histopathological images and genomic data (*PAGE-Net*). For model interpretation, a focus is put on the pathology-specific layers and the genome-specific layers. For the genome-specific layers, pathway-based ranking based on partial derivatives is applied and analyzed analogously to *Cox-PASNet* to identify genetic patterns that cause different survival rates between patients. From pathology-specific layers, pre-identified histopathological patterns associated to cancer survival are displayed by means of survival-discriminative feature maps. The feature maps reveal whether the model successfully identifies the morphological patterns that are of interest to pathologists. Furthermore they can uncover previously undetected relationships between any specific morphological patterns and survival prognosis. Like Hao et al.³¹ Zhao et al.⁹⁰ aim to integrate multi-omics data into an interpretable survival deep learning framework with *DeepOmix*. *DeepOmix* is a feed-forward neural network. Again, key to the intrinsic interpretability of the model is the incorporation of prior biological knowledge of gene functional module networks in a functional module layer. Such functional module networks may for instance be tissue networks, gene co-expression networks, or prior biological signaling pathways. While the hidden layers are able to capture the nonlinear and hierarchical effects of biological pathways associated with survival time, purposefully, low-dimensional representations are learned in the functional module layer, such that nodes represent groups of patients. Significant modules corresponding to prognostic prediction results are extracted by ranking them based on p-values obtained by a Kolmogorov-Smirnov test. It assesses whether the distribution of the patients in the gene modules is significantly different from previously defined high-risk/low-risk subgroups based on predicted survival time. In *Cox-nnet*⁹¹ interpretability is derived by first selecting the most important nodes based on the highest variances in contribution. Contribution is calculated as the output value of each hidden node weighted by the corresponding coefficient of a Cox regression output layer. A t-SNE plot visualization reveals the hidden nodes' ability to reduce dimensionality of the initial omics data while effectively distinguishing samples based on their prognostic index. Then, to explore the biological relevance of the previously discerned important hidden nodes significantly enriched gene pathways are identified using Pearson's correlation between the log transformed gene expression input and the output score of each node across all patients. To obtain an importance score of each input gene for survival outcome prediction, the average partial derivative of the output of the model with respect to each input gene value across all patients is computed.

For other methods, interpretability serves as an incidental consequence of an intrinsic design element within the novel neural network architecture proposed and is only briefly addressed in a peripheral manner. *SurvTRACE*⁹², a transformer-based deep

learning model for competing risk survival analysis, uses multi-head self-attention in the encoder module allowing the model to automatically learn high-order feature interactions. Additionally, the learned attention scores can be utilized to understand feature relevance, interactions and importance. *SurvNode*⁹³, a deep learning framework for multi-state modelling, utilizes latent variable extensions to model uncertainty. The resulting latent space is divided into clusters, ideally providing a meaningful differentiation between survival outcomes and state transitions. Groha et al. choose to plot the state occupation probabilities, estimated using the non-parametric Aalen–Johansen estimator, for each cluster separately over time. An alternative method for acquiring feature effects linked to each cluster is introduced, fitting a logistic surrogate regression model within each individual cluster.

3 | REAL DATA APPLICATION

The primary motivation behind the methodologies discussed in this paper lies in the generation of explanations for different types of survival models. These explanations play a crucial role in interpreting and comprehending pivotal model decisions, ideally contributing to uncovering novel universal domain specific knowledge. In order to demonstrate a potential use, we employ several of the discussed interpretable machine learning techniques on four models trained with real-world data sourced from the Demographic and Health Survey of the US-Agency for International Development (US-AID)⁹⁴. The focal objective is to predict the under-5 year survival time of children in Ghana in 2014, leveraging a set of 12 demographic, medical, and socio-economic features. A descriptive overview table detailing the features of interest can be found in the appendix (see Table 1 in Appendix A).

3.1 | Data Preprocessing and Exploratory Analysis

The final analysis dataset consists of 7743 children. Of the twelve selected features, two contain missing values, the place of delivery of the child (`place_delivery`) (1874 missing) and the reported DPT 1 vaccination status (`dpt1_vaccination`) (1916 missing), which are imputed by single imputation with predictive mean matching for simplicity. The survey includes mothers between the ages of 15 and 49, who report the ages of their children in months born in the last five years. If the child is alive, their age in months at the time of the questionnaire is reported. If the child is dead, their age at the time of death is recorded in months, only if the child was below two years old. If the child was older than 24 months at the time of death, the age is rounded to the next full year, which is reflected in the distribution of the survival times of the dead children in the sample, shown in figure 1a. In the sample, a substantial proportion of fatalities are stillbirths (> 750), some events occur at any timepoint between 0-20 months, with a peak at 12 months due to rounding effects. For the deaths recorded at ages ≥ 24 a decrease in magnitude is observed. This pattern is mirrored in the Kaplan–Meier survival curve in Figure 1b, which decreases stepwise at $t = 0, 12, 24, 36, 48, 60$. Children are censored if they are alive and their age is reported to be below 60 months. In total 5595 children are censored. The distribution of the survival time (Figure 1a) in the group of living children (without event) is approximately uniform.

3.2 | Model Fitting and Evaluation

The Cox proportional hazards model is fit to the data as a baseline and compared to three popular machine learning models for survival analysis: a random survival forest model (`ranger` from `ranger` package), gradient boosting with survival trees (`blackboost` from `mboost` package) and a *DeepSurv* survival neural network (`deepsurv` from the `survivalmodels` package). The data is split into training, validation and test set and the validation set is used to perform hyperparameter tuning for the machine learning models using 10-fold cross-validation. The performance is then evaluated and the explainability techniques are applied to the test data. The performance measures in Table 2a shows that the `blackboost` model performs best in terms of integrated Brier score and C-index, directly followed by the `ranger` model, while the `coxph` model is calibrated the best

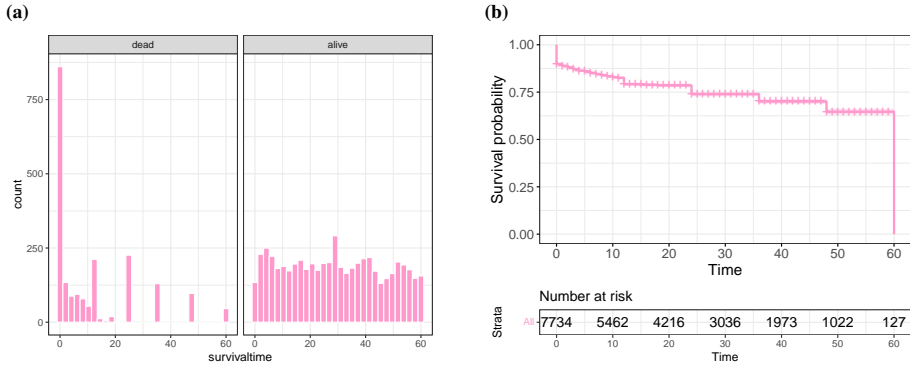


FIGURE 1 Exploratory analysis of survival data of children under 5 in the DHS dataset. (a) shows the survival time distributions conditional on survival status. (b) depicts the Kaplan-Meier survival curve and risk sets.

according to the D-calibration score. Overall, all models perform reasonably well on the data. From the Brier score performance plot over time, we can see that the prediction performance heavily decreases for children aged > 55 months due to the relatively small number of individuals at risk as well as the low number of events between 55 and 60 months.

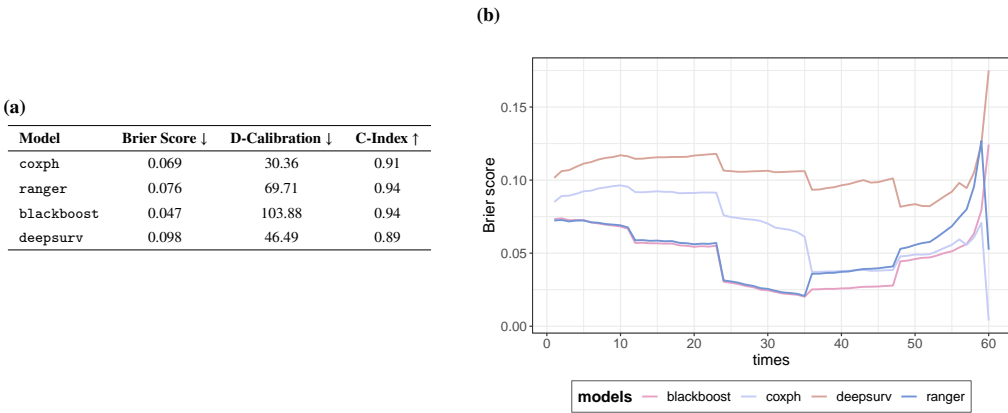


FIGURE 2 Performance comparison of survival models. In table (a) the integrated Brier score is utilized as a scoring rule to quantify if the probabilistic predictions are close to the true values. D-calibration serves as a calibration measure to quantify if the average prediction is close to the truth. As a discrimination measure, C-index is used, which quantifies if a model correctly identifies if one observation is at a higher risk than another. Figure (b) shows the Brier score at different timepoints.

3.3 | Application of Interpretable Machine Learning Methods

In the following, the interpretable machine learning methods discussed in the methodological section of the paper are applied to the four models estimated on the DHS under-5 year mortality data (see Section 3.2). The purpose of this section is to provide exemplary illustrations of the methods as a basic guideline for researchers aiming to gather insights into (machine learning) survival models. Most explanations were generated using the `survex`⁹⁵ package in R, the code to reproduce the results can be found on Github: https://github.com/sophhan/IMLSA_2024.

3.3.1 | Permutation Feature Importance

Permutation feature importance is used to provide highly compressed, global insights into a models' behaviors. The plots in Figure 3 show the increase in Brier score loss at every timepoint $t = 0, \dots, 59^4$ when replacing a feature with its permuted version for the `coxph` and the `blackboost` model. For both models, `dpt1_vaccination` and `total_dead_sons` are the two most important features. While the performance of `coxph` model relies heavily on the `dpt1_vaccination` feature in particular for increasing survival times, for the `blackboost` model, the consequential error increase of permuting `dpt1_vaccination` is less strong in absolute magnitude. Likewise, the difference in importance of `dpt1_vaccination` compared to other important features is much smaller in absolute magnitude in the `blackboost` model compared to the `coxph` model; at times the importance of the `total_dead_sons` feature actually overtakes `dpt1_vaccination` in absolute increase of Brier score loss. The correlation structure depicted in the appendix in Figure 10 does not suggest that the `blackboost` model wrongly attributes some of the importance of the `dpt1_vaccination` feature to other features such as `total_dead_sons`, but rather that its not accurately reflected by the `coxph` model.

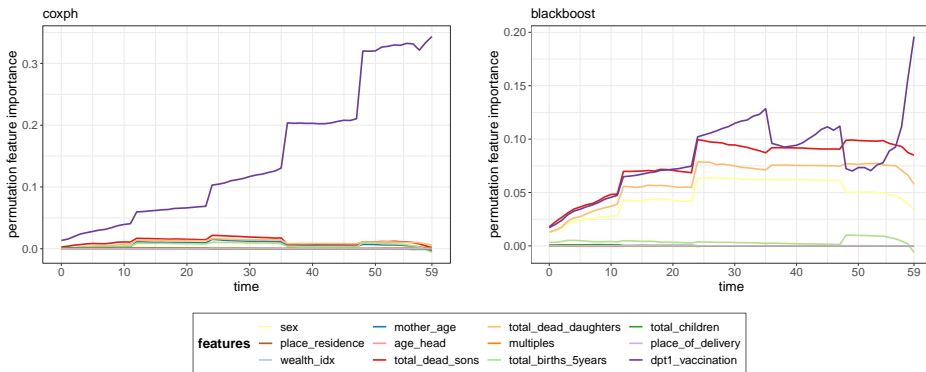


FIGURE 3 Permutation feature importance for the `coxph` model (left) and the `blackboost` model (right). The y-axis denotes the Brier score loss after permutations of each separate feature with the loss of the full model including all features without permutations subtracted. The `coxph` model relies heavily on the `dpt1_vaccination` feature in particular for predicting higher survival times. In `blackboost`, predictive power is distributed more evenly between `dpt1_vaccination`, `total_dead_sons`, `total_dead_daughters` and `sex`.

⁴ $t = 60$ is disregarded due to the poor performance across models to avoid confusion.

3.3.2 | Individual Conditional Expectation and Partial Dependence Plots

Now centered individual conditional expectation (c-ICE) and partial dependence plots (c-PDP) are jointly plotted to visualize the influence of the `mother_age` feature on the probability of survival of children in the test set at different ages (see Figure 4). To compute the c-ICE curves, a random sample of 100 children is taken from the test set, to ensure discernability of the depicted c-ICE curves by avoiding over-cluttering. The c-PDP curves are computed on the full test set. Centering with regard to the minimum observed feature value is employed to facilitate the assessment of the degree of heterogeneity in the ICE curve shapes to determine whether there are interactions between `mother_age` and other features. For additional visual clarity, the c-ICE curves are plotted without the c-PDPs in Figure 11 in the appendixA. For both the `ranger` and `deepsurv` models, the degree of heterogeneity in the c-ICE curves is low to moderate compared across different individuals, yet increasing in prevalence for higher survival times. This suggests a low to moderate degree of interaction between the `mother_age` feature and other features in both presented models. Considering the c-PDPs, the average predicted probability of survival is found to decrease in both models as the ages of mothers increase. In both models, this effect becomes stronger as children become older. However, the magnitude of this observed effect differs greatly between the two models. In the `ranger` model, the age of the mother does not affect the average predicted probability of survival of the model up until the age of about 35 years. The negative effect on the average predicted probability of survival for child ages > 35 months is also rather small in absolute magnitude, not exceeding a change in -0.05 percentage points, rendering the effect of the age of the mother on their child's survival probability estimated by `ranger` immaterial. In contrast, `deepsurv` attributes a sizeable influence of the mother's age on their child's predicted probability of survival, for instance for children aged 59 months, the change in average predicted probability of survival is predicted to increase in absolute magnitude from -0.05 to -0.35 percentage points.

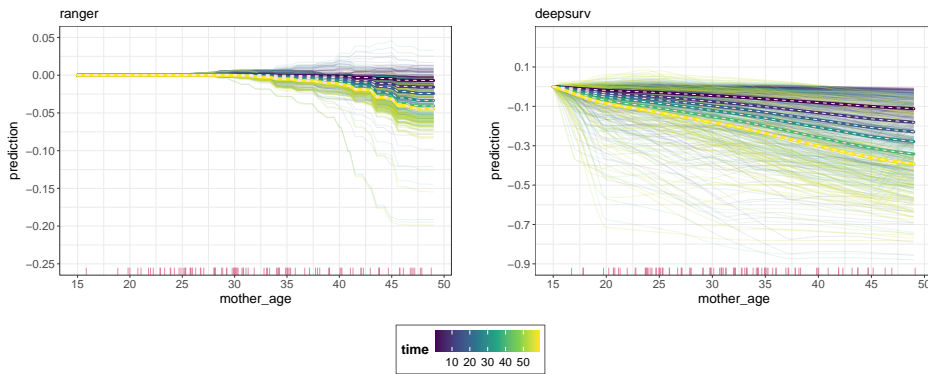


FIGURE 4 c-ICE and c-PDP curves for the `ranger` model (left) and the `deepsurv` model (right) for the `mother_age` feature. c-ICE curves are depicted as thin colored lines, while c-PDPs are thick colored lines with white dashed lines in the center. Different colors indicate different survival times, i.e. child ages. The pink rug on the x-axis shows the feature distribution across the sampled children. The c-ICE (c-PD) curves depict the (average) predicted probability of survival for changes in the values of the feature of interest, denoted on the x-axis. In both models, higher `mother_age` values are in general associated with a lower predicted probability of survival, with the effect amplifying as children get older.

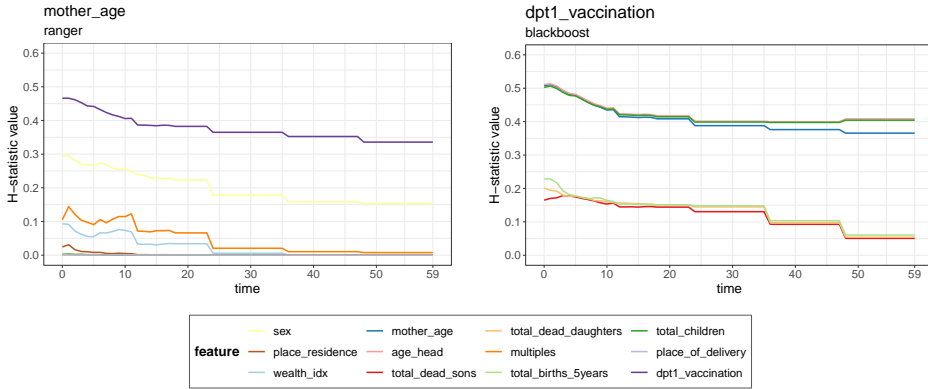


FIGURE 5 The 2-way interaction strengths ($H_{jk}(t)$ -statistics) curves for the `ranger` model (left) and the `blackboost` model (right) for the `mother_age` and the `dpt1_vaccination` feature, respectively. The interaction at each timepoint is the proportion of variance explained by the interaction. The `dpt1_vaccination` feature is found to interact moderately strong with other features in both models.

3.3.3 | H-statistics

Complementary to the previous results, we calculate the two-way interaction statistics for the `mother_age` and the `dpt1_vaccination` feature in the `ranger` and `blackboost` models, respectively (see Figure 5). Note that for any model, that does not allow for any feature interactions, such as the `coxph`, the H-statistics will be 0 at any given timepoint, if computed on the full test sample. As deduced from the low to moderate degree of heterogeneity visible in the c-ICE curves generated from the `ranger` model for the `mother_age` feature in Figure 11, the values of the $H_{jk}(t)$ -statistics are considerably high for only two features (`dpt1_vaccination` and `sex`). The strongest interactions over time for `dpt1_vaccination` in the `blackboost` model are with `mother_age`, `age_head` and `total_dead_children`. Note that for categorical features of interest, the corresponding $H_{jk}(t)$ statistics can only be computed for continuous features. For both the `ranger` and `blackboost` model, the strength of the depicted interaction measures decreases over time. Generally speaking, the H-statistic values can always only be an indication of interaction strength; it is difficult to say when it is large enough to consider an interaction strong, relevant interactions need to be assessed using alternative methods to determine type and direction of interaction.

3.3.4 | Accumulated Local Effects

Since interactions with other features cannot be ruled out in the machine learning models for the `dpt1_vaccination` in particular, it is interesting to consider accumulated local effects (ALE) plots instead of PDPs, as they can be biased. The uncentered ALE main effect curves for the `dpt1_vaccination` feature computed on the full test set for the `coxph` and `blackboost` model are shown in Figure 6. Their interpretation is analogous to uncentered PDPs, except that the effect of different feature values on the average predicted survival probability at different survival time points is computed conditional on a given value. The feature values "don't know" and "vaccination marked on card" are excluded due to an insufficient amount of observations (see Figure 1), because they lead to unreliable effect estimates. Both models predict the average probability of survival of children with a positive vaccination status (either "reported by mother" or "vaccination date on card") to be higher than the average predicted probability of survival of children without vaccination ("no"). In the `blackboost` model, this difference decreases for increasing ages. The magnitude of the estimated ALE main effects for the `coxph` model reflects the high reliance of the model on this feature for

prediction, as discussed in Section 3.3.1. In both cases, the temporal pattern follows that of the Kaplan-Meier estimator induced by deaths being recorded only at full ages for children above the age of 12 months (see Figure 1b). The highest average survival probability is predicted for the "child older than 3 years" category. This is an artificially created category resulting from the DPT1 vaccination status being recorded only for children below the age of 3 years. Thus, it is to be expected by design that the predicted survival probability of children whose DPT1 vaccination status is known, is on average comparably lower to that of children older than 3 years. Since there is no training data on children's DPT1 vaccination status available for children > 36 months, the ALE estimates are not reliable in the respective categories for this age range. Note, that this is an extreme case of a universal issue to consider for regions with few available observations. In general, an explanation can only ever be as reliable as the model it explains.

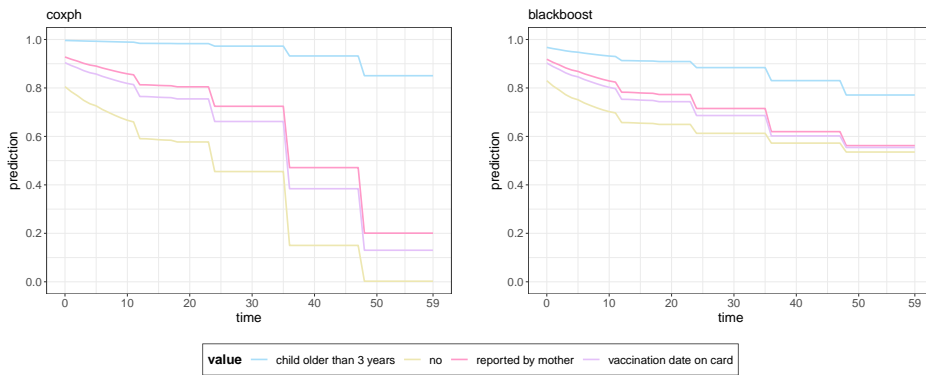


FIGURE 6 Accumulated local effects curves for the `dpt1_vaccination` feature in the `coxph` model (left) and the `blackboost` model (right). The accumulated local effects are plotted over different survival times as unbiased estimates of the main effects of the different values of the categorical `dpt1_vaccination` feature. Both models predict a higher average survival probability for children with a positive vaccination status than for those without vaccination.

3.3.5 | SurvLIME

After exploring the global effects of features and their interactions on the predicted survival of the children, we will now demonstrate how different local methods can be utilized to explore the effects of certain features on one specific instance. For this purpose two exemplary children are chosen from the test set, whose characteristics are denoted in Table 2. For these children *SurvLIME* is applied to the black box survival curves predicted by the *ranger* model. These curves are shown in Figure 12 alongside the survival curve predictions of the Cox proportional hazard surrogate model in the neighborhood⁵ of the respective observation of interest. Figure 7 shows the local importance values estimated based on the surrogate model, ordered based on absolute effect size, with zero coefficients excluded. For both children the locally important features deviate significantly from the globally important features permutation feature importance (see Figure 3) or global *SurvSHAP(t)* importance (see Figure 9). The local importance values can for instance be interpreted in the following way: The age of the mother positively influences the predicted probability of survival of the surrogate model for child C1, while it strongly negatively affects the predicted probability of survival for child C2; the same holds for the *age_head* feature in both cases. It must be brought to the fore, that the *SurvLIME* explanation survival function diverges strongly from the black box survival prediction for C1, indicating a rather poor fit of the surrogate model (compare in Figure 12); while the divergence is less strong for the curves of C2, the fit is still subpar. In conclusion, the lack of a theoretical foundation, as well as the many practical problems in *SurvLIME* estimation, such as the correct definition of the sampling neighborhood, the overall instability of explanations and the inability to capture time dependent effects arguably hinders practical usability of *SurvLIME* explanations.

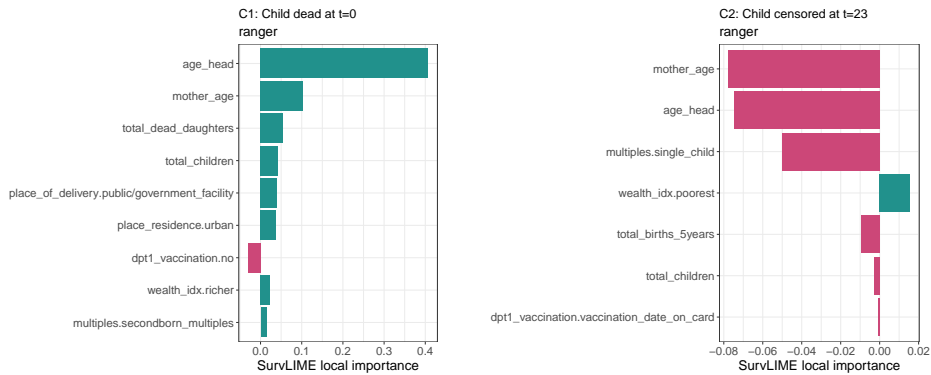


FIGURE 7 The local feature importance values from *SurvLIME* for two selected observations computed on the *ranger* model ranked by absolute magnitude. The local importance values of each feature are obtained as the product of the absolute values of the coefficients estimated by the respective surrogate Cox Proportional Hazards model model and the feature values observed for the specific observation. Categorical features are one-hot encoded, with the positive value chained after the feature name.

⁵By default the neighborhood size is set to $g = 100$.

3.3.6 | SurvSHAP(t)

In contrast to *SurvLIME*, *SurvSHAP(t)* offers insight into how each feature influences the black box survival function at different timepoints. For comparison purposes the same children as described in Table 2. A general juxtaposition of locally important features identified by *SurvLIME* (Figure 7) vs. *SurvSHAP(t)* (Figure 8) shows that they do not generally align, with the exception of the `total_dead_daughters` feature for child C1. Furthermore, *SurvSHAP(t)* further highlights the inadequacy of *SurvLIME* as an explanation method, as the plots in Figure 8 show that the relative importance of different features is variable over time, even changing in relative order. In general, the *SurvSHAP(t)* values at different timepoints quantify the contribution of each feature to the difference between the black box survival function for the particular child and the average predicted survival function of the black box. For the child dead at $t = 0$ (C1), the mother having two deceased daughters, having no births in the 5 previous years and the child having no `dpt1_vaccination` most strongly negatively contribute to the difference between the average predicted survival curve and the black box survival curve estimated by the `ranger` model shown in Figure 12. In contrast, for the child censored at $t = 23$ (C2), the absence of any deceased sons or daughters as well as the mother having birthed one child in the previous 5 years are the three features most important for explaining why the predicted survival curve for this child exceeds the average predicted survival curve of the black box model.

SurvSHAP(t) values can also help to reveal the impact of each feature across the entire dataset, highlighting which features consistently contribute more or less to the predictions. On the left hand side Figure 9 shows the average absolute *SurvSHAP(t)* contributions over time for the `ranger` model; `total_dead_sons` is the most important feature at every timepoint, followed by `dpt1_vaccination`, which remains the second most important feature up until $t = 20$, where it is overtaken by `total_dead_daughters` and eventually at $t \approx 45$ also by `total_births_5years`. In order to understand both importance and direction of feature contributions aggregated over time for all observations in the test set beeswarm plots, as depicted on the right-hand side of Figure 9, can be used as information-dense summaries. For less important features, such as `total_children` the dots representing the aggregates *SurvSHAP(t)* values are closely scattered around zero, whereas for more influential features, the dots are spread out along the x-axis. Color is used to display the original value of a feature, to reveal their association with the aggregated *SurvSHAP(t)* values. For instance, observations with low values of the `total_dead_sons` and `total_dead_daughters` features are in most cases associated with positive aggregated *SurvSHAP(t)* contributions, meaning they make a positive contribution to the predicted probability of survival of each instance.

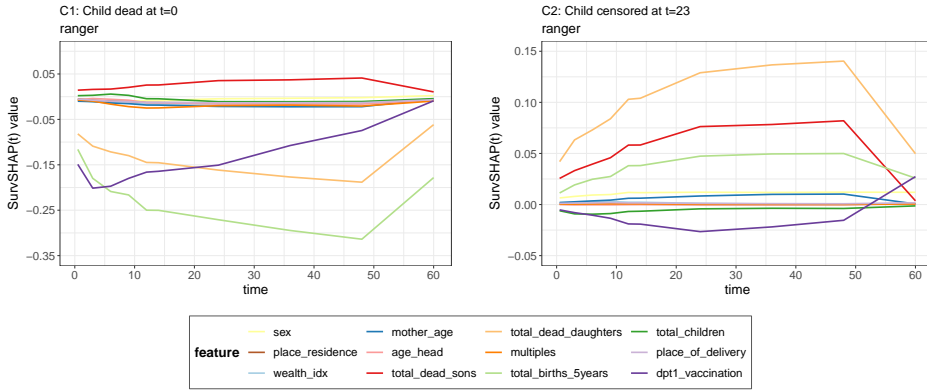


FIGURE 8 Aggregated *SurvSHAP(t)* results computed on the *ranger* model. The left plot shows the average absolute *SurvSHAP(t)* values computed over all observations in the test set plotted at different timepoints t to quantify the global importance of each feature over time. The two right-hand side figures are beeswarm plots of the *SurvSHAP(t)* values of every observation aggregated over time for a selected subset of features to summarize the global effect of individual features on the predicted survival probability.

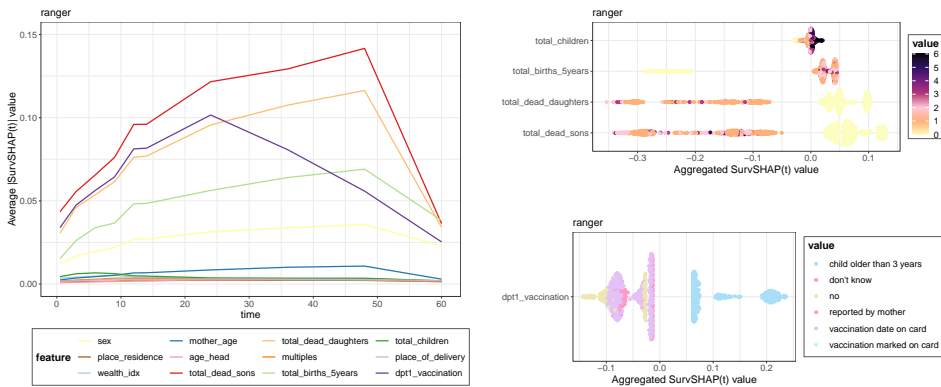


FIGURE 9 *SurvSHAP(t)* for two selected observations computed on the *ranger* model. The *SurvSHAP(t)* values plotted at different timepoints t quantify the contribution of each feature to the difference between the black box survival function predicted for the particular observation and the average predicted survival function of the black box; hence all curves summed up over the different timepoints added to the average predicted survival curve of the model, will output the predicted survival curve of the chosen observation.

4 | CONCLUSION

This comprehensive review and tutorial paper aims to serve as a fundamental reference for researchers delving into survival interpretable machine learning. Emphasis is put on model-agnostic methods for their applicability in a broad modelling context and their consequential ease of adaption into accessible software. We review existing work on model-agnostic interpretable machine learning methods specifically developed for survival analysis, including survival counterfactuals, *SurvLIME* and its extensions, *SurvSHAP* and *SurvSHAP(t)*. Immediate research gaps identified are addressed, as other popular model-agnostic methods, which prior to this paper have not yet been modified to work in the survival context, are formally adapted to survival analysis. This concerns methods, whose scope of adjustment do not warrant uniquely dedicated pieces of work, such as ICE, PDP, ALE, H-statistic or different feature importance measures. By unifying the formalization of existing and newly adapted survival explainability methods, a concise referential basis is created, on which new work can be built upon. Furthermore, it facilitates highlighting limitations known from the non-functional output setting, as well as additional deficiencies resulting from the unique properties of the survival setting. In the process, opportunities for future research are identified and outlined. In addition to model-agnostic methods, the paper explores existing model-specific interpretability methods, particularly in the domains of survival tree ensemble learners and survival neural networks, overall offering a thorough overview of the current state of research in the field of interpretable machine learning for survival analysis.

An overarching challenge emerging from the discussion on explainability for survival analysis is visualization. Visualization and interpretability are inseparably intertwined, as it is an indispensable tool to deliver human-understandable results. As survival models typically deliver functional outcomes dependent on time, survival explanations and resulting visualizations usually require at least one additional dimension, compared to their counterparts in a classic, non-functional output setting. Balancing a comprehensive presentation of results with transparency and cognitive intelligibility for humans, is a central challenge for future research in the field of interpretability for survival analysis or interpretability of functional output problems in general. In this paper, we have also discussed shortcomings of more traditional means of making survival models interpretable, such as hazard ratios. The tendency to collapse results into single numbers, such as hazard ratios, restricted mean survival time or median survival time, is arguably an attempt of making their complexity comprehensible for users, at the apparent cost of a loss of important information. For real transparency and responsibility, a way must be found in which complex results are not simply reduced, but can be presented such that they deliver insights not erasing their nuances, while remaining comprehensible for end users and practitioners, e.g. in the medical domain. This has to be jointly addressed by developing and deploying a broader and universally applicable spectrum of explainability methods for survival data, as well as more acute and insightful visualizations of existing methods and results.

Moreover, the paper includes an application of some of the reviewed and newly-adapted interpretability methods to real data, for the purpose of gaining insights into a set of statistical and machine learning models predicting the under-5 year mortality of children in Ghana. This part is meant to serve as a tutorial or guide for researchers, on how the methods can be utilized in practice to facilitate understanding of why certain decisions or predictions are made by the models. The computational results are obtained from the *survex* package, a user-friendly, state-of-the-art R software package, which allows to produce explanations for survival models from numerous of the most popular survival analysis related packages in R.⁹⁵ Since the analysis is heavily simplified for the sake of clarity and the models are explicitly framed as prediction tools, conclusions about the underlying data must be drawn with utmost care. Particularly, it is crucial to highlight, that statements about causal relationships can in general not be made from explanation results, since the underlying models, like most statistical learning procedures merely analyze correlation structures between features instead of the true inherent causal structure of the data generating process.⁹⁶ In summary, it needs to be stressed, that interpretable machine learning methods are useful to discover knowledge, to debug or justify, as well as control and improve models and their predictions, but not to make causal interpretations of the data.⁹⁶

Future work could improve existing interpretability methods with large potential in the survival field, like survival counter-

factuals, feature decomposition or Shapley values. Additionally, we encourage researchers to rethink interpretability in the context of censored data or data with functional outcomes, developing novel methods targeted to the unique needs and requirements in these areas. So far, the existing methods are only available for standard right-censored survival data, hence explainability for non-standard censoring or competing risk settings, are likewise a direction for future work.

REFERENCES

1. Cox DR. Regression models and life-tables. *Journal of the Royal Statistical Society: Series B (Methodological)* 1972; 34(2): 187–220.
2. Rulli E, Ghilotti F, Biagioli E, et al. Assessment of proportional hazard assumption in aggregate data: a systematic review on statistical methodology in clinical trials using time-to-event endpoint. *British Journal of Cancer* 2018; 119(12): 1456–1463. doi: 10.1038/s41416-018-0302-8
3. Martinussen T, Vansteelandt S. On collapsibility and confounding bias in Cox and Aalen regression models. *Lifetime Data Analysis* 2013; 19(3): 279–296. doi: 10.1007/s10985-013-9242-z
4. Martinussen T. Causality and the Cox regression model. *Annual Review of Statistics and Its Application* 2022; 9: 249–259. doi: <https://doi.org/10.1146/annurev-statistics-040320-114441>
5. Wang P, Li Y, Reddy CK. Machine learning for survival analysis: A survey. *ACM Computing Surveys (CSUR)* 2019; 51(6): 1–36. doi: <https://doi.org/10.1145/3214306>
6. Ishwaran H, Kogalur UB, Blackstone EH, Lauer MS. Random survival forests. *The Annals of Applied Statistics* 2008; 2(3): 841 – 860. doi: 10.1214/08-AOAS169
7. Hothorn T, Bühlmann P, Dudoit S, Molinaro A, Van Der Laan MJ. Survival ensembles. *Biostatistics* 2006; 7(3): 355–373.
8. Katzman JL, Shaham U, Cloninger A, Bates J, Jiang T, Kluger Y. DeepSurv: personalized treatment recommender system using a Cox proportional hazards deep neural network. *BMC Medical Research Methodology* 2018; 18(1): 1–12.
9. Lee C, Zame W, Yoon J, Van Der Schaar M. Deephit: A deep learning approach to survival analysis with competing risks. In: . 32. ; 2018.
10. Zhao L, Feng D. DNNSurv: Deep Neural Networks for Survival Analysis Using Pseudo Values.; 2020
11. Ahmad MA, Eckert C, Teredesai A. Interpretable machine learning in healthcare. In: BCB '18. Association for Computing Machinery; 2018; New York, NY, USA: 559–560
12. Vellido A. The importance of interpretability and visualization in machine learning for applications in medicine and health care. *Neural computing and applications* 2020; 32(24): 18069–18083. doi: <https://doi.org/10.1007/s00521-019-04051-w>
13. Chen IY, Szolovits P, Ghassemi M. Can AI help reduce disparities in general medical and mental health care?. *AMA journal of ethics* 2019; 21(2): 167–179. doi: 10.1001/amajethics.2019.167
14. Manrai AK, Funke BH, Rehm HL, et al. Genetic misdiagnoses and the potential for health disparities. *New England Journal of Medicine* 2016; 375(7): 655–665. doi: 10.1056/NEJMs1507092
15. Mhasawade V, Zhao Y, Chunara R. Machine learning and algorithmic fairness in public and population health. *Nature Machine Intelligence* 2021; 3(8): 659–666. doi: <https://doi.org/10.1038/s42256-021-00373-4>
16. Rajkomar A, Hardt M, Howell MD, Corrado G, Chin MH. Ensuring fairness in machine learning to advance health equity. *Annals of internal medicine* 2018; 169(12): 866–872. doi: 10.7326/M18-1990
17. Gianfrancesco MA, Tamang S, Yazdany J, Schmajuk G. Potential biases in machine learning algorithms using electronic health record data. *JAMA internal medicine* 2018; 178(11): 1544–1547. doi: 10.1001/jamainternmed.2018.3763

18. Barraón E, Barraón L. Effect of right censoring bias on survival analysis.; 2020.
19. Bland JM, Altman DG. The logrank test. *Bmj* 2004; 328(7447): 1073.
20. Schulman KA, Berlin JA, Harless W, et al. The effect of race and sex on physicians' recommendations for cardiac catheterization. *New England Journal of Medicine* 1999; 340(8): 618–626.
21. Krzyżiński M, Spytek M, Baniecki H, Biecek P. SurvSHAP (t): Time-dependent explanations of machine learning survival models. *Knowledge-Based Systems* 2023; 262: 110234. doi: <https://doi.org/10.1016/j.knosys.2022.110234>
22. Molnar C. *Interpretable Machine Learning*. 2 ed. 2022.
23. Kovalev MS, Utkin LV, Kasimov EM. SurvLIME: A method for explaining machine learning survival models. *Knowledge-Based Systems* 2020; 203: 106164. doi: <https://doi.org/10.1016/j.knosys.2020.106164>
24. Alabdallah A, Pashami S, Rögnavaldsson T, Ohlsson M. SurvSHAP: A proxy-based algorithm for explaining survival models with SHAP. In: *IEEE*. ; 2022: 1–10
25. Kovalev M, Utkin L, Coolen F, Konstantinov A. Counterfactual explanation of machine learning survival models. *Informatica* 2021; 32(4): 817–847. doi: <https://doi.org/10.15388/21-INFOR468>
26. Utkin LV, Satyukov ED, Konstantinov AV. SurvNAM: The machine learning survival model explanation. *Neural Networks* 2022; 147(C): 81–102. doi: [10.1016/j.neunet.2021.12.015](https://doi.org/10.1016/j.neunet.2021.12.015)
27. Utkin LV, Zaborovsky VS, Kovalev MS, Konstantinov AV, Politaeva NA, Lukashin AA. Uncertainty interpretation of the machine learning survival model predictions. *IEEE Access* 2021; 9: 120158-120175. doi: [10.1109/ACCESS.2021.3108341](https://doi.org/10.1109/ACCESS.2021.3108341)
28. Rahman MM, Purushotham S. PseudoNAM: A pseudo value based interpretable neural additive model for survival analysis. In: *CEUR*; 2021
29. Xu L, Guo C. CoxNAM: An interpretable deep survival analysis model. *Expert Systems with Applications* 2023; 227: 120218. doi: <https://doi.org/10.1016/j.eswa.2023.120218>
30. Hao J, Kosaraju SC, Tsaku NZ, Song DH, Kang M. PAGE-Net: interpretable and integrative deep learning for survival analysis using histopathological images and genomic data. In: *World Scientific*. ; 2019: 355–366
31. Hao J, Kim Y, Mallavarapu T, Oh JH, Kang M. Interpretable deep neural network for cancer survival analysis by integrating genomic and clinical data. *BMC medical genomics* 2019; 12(10): 1–13.
32. Bharati S, Mondal MRH, Podder P. A review on explainable artificial intelligence for healthcare: Why, how, and when?. *IEEE Transactions on Artificial Intelligence* 2023. doi: [10.1109/TAI.2023.3266418](https://doi.org/10.1109/TAI.2023.3266418)
33. Srinivasu PN, Sandhya N, Jhaveri RH, Raut R. From blackbox to explainable AI in healthcare: existing tools and case studies. *Mobile Information Systems* 2022; 2022: 1–20. doi: <https://doi.org/10.1155/2022/8167821>
34. Nazar M, Alam MM, Yafi E, Su'ud MM. A systematic review of human–computer interaction and explainable artificial intelligence in healthcare with artificial intelligence techniques. *IEEE Access* 2021; 9: 153316–153348. doi: [10.1109/ACCESS.2021.3127881](https://doi.org/10.1109/ACCESS.2021.3127881)
35. Alex Goldstein JB, Pitkin E. Peeking inside the black box: Visualizing statistical learning with plots of individual conditional expectation. *Journal of Computational and Graphical Statistics* 2015; 24(1): 44–65. doi: <https://doi.org/10.1080/10618600.2014.907095>
36. Wachter S, Mittelstadt B, Russell C. Counterfactual explanations without opening the black box: Automated decisions and the GDPR. *Harvard Journal of Law & Technology* 2017; 31: 841–887. doi: <https://doi.org/10.48550/arXiv.1711.00399>
37. Eberhart R, Kennedy J. Particle swarm optimization. In: . 4. Citeseer. ; 1995: 1942–1948
38. Dandl S, Molnar C, Binder M, Bischl B. Multi-objective counterfactual explanations. In: *Springer*. Springer-Verlag; 2020; Berlin, Heidelberg: 448–469

39. Utkin LV, Kovalev MS, Kasimov EM. SurvLIME-Inf: A simplified modification of SurvLIME for explanation of machine learning survival models.; 2020
40. Kovalev MS, Utkin LV. A robust algorithm for explaining unreliable machine learning survival models using the Kolmogorov–Smirnov bounds. *Neural Networks* 2020; 132: 1–18.
41. Lundberg SM, Lee SI. A unified approach to interpreting model predictions. In: . 30 of *NIPS'17*. Curran Associates Inc.; 2017; Red Hook, NY, USA: 4768–4777
42. Ter-Minassian L, Ghalebikesabi S, Diaz-Ordaz K, Holmes C. Explainable AI for survival analysis: A median-SHAP approach.; 2024
43. Shapley LS. *17. A Value for n-Person Games*: 307–318; Princeton: Princeton University Press . 1953
44. Lundberg SM, Erion G, Chen H, et al. From local explanations to global understanding with explainable AI for trees. *Nature Machine Intelligence* 2020; 2(1): 56–67. doi: <https://doi.org/10.1038/s42256-019-0138-9>
45. Olsen LHB, Glad IK, Jullum M, Aas K. A comparative study of methods for estimating conditional Shapley values and when to use them.; 2023
46. Aas K, Jullum M, Løland A. Explaining individual predictions when features are dependent: More accurate approximations to Shapley values. *Artificial Intelligence* 2021; 298: 103502. doi: <https://doi.org/10.1016/j.artint.2021.103502>
47. Olsen LH, Glad IK, Jullum M, Aas K. Using Shapley values and variational autoencoders to explain predictive models with dependent mixed features. *Journal of Machine Learning Research* 2022; 23(213): 9553–9603. doi: <https://doi.org/10.48550/arXiv.2111.13507>
48. Simonyan K, Vedaldi A, Zisserman A. Deep inside convolutional networks: Visualising image classification models and saliency maps. In: ; 2014
49. Shrikumar A, Greenside P, Kundaje A. Learning important features through propagating activation differences. In: . 70. PMLR. ; 2017: 3145–3153
50. Smilkov D, Thorat N, Kim B, Viégas F, Wattenberg M. SmoothGrad: Removing noise by adding noise.; 2017
51. Bach S, Binder A, Montavon G, Klauschen F, Müller KR, Samek W. On pixel-wise explanations for non-linear classifier decisions by layer-wise relevance propagation. *PLoS one* 2015; 10(7): e0130140. doi: 10.1371/journal.pone.0130140
52. Cho HJ, Shu M, Bekiranov S, Zang C, Zhang A. Interpretable meta-learning of multi-omics data for survival analysis and pathway enrichment. *Bioinformatics* 2023; 39(4): btad113. doi: 10.1093/bioinformatics/btad113
53. Sundararajan M, Taly A, Yan Q. Axiomatic attribution for deep networks.; 2017. arXiv:1703.01365 [cs]
54. Selvaraju RR, Cogswell M, Das A, Vedantam R, Parikh D, Batra D. Grad-cam: Visual explanations from deep networks via gradient-based localization. In: IEE; 2017: 618–626
55. Fong RC, Vedaldi A. Interpretable explanations of black boxes by meaningful perturbation. In: IEE; 2017: 3429–3437
56. Springenberg JT, Dosovitskiy A, Brox T, Riedmiller M. Striving for simplicity: The all convolutional net.; 2015
57. Erion G, Janizek JD, Sturmfels P, Lundberg SM, Lee SI. Improving performance of deep learning models with axiomatic attribution priors and expected gradients. *Nature Machine Intelligence* 2021; 3(7): 620–631. doi: 10.1038/s42256-021-00343-w
58. Friedman JH. Greedy Function Approximation: A Gradient Boosting Machine. *The Annals of Statistics* 2001; 29(5): 1189–1232.
59. Apley DW, Zhu J. Visualizing the effects of predictor variables in black box supervised learning models. *Journal of the Royal Statistical Society Series B: Statistical Methodology* 2020; 82(4): 1059–1086. doi: 10.1111/rssb.12377
60. Breiman L. Random forests. *Machine learning* 2001; 45: 5–32. doi: <https://doi.org/10.1023/A:1010933404324>

61. Lei J, G'Sell M, Rinaldo A, Tibshirani RJ, Wasserman L. Distribution-free predictive inference for regression. *Journal of the American Statistical Association* 2018; 113(523): 1094–1111. doi: <https://doi.org/10.1080/01621459.2017.1307116>
62. Strobl C, Boulesteix AL, Kneib T, Augustin T, Zeileis A. Conditional variable importance for random forests. *BMC Bioinformatics* 2008; 9(307): 1–11. doi: <https://doi.org/10.1186/1471-2105-9-307>
63. Hooker G, Mentch L, Zhou S. Unrestricted permutation forces extrapolation: variable importance requires at least one more model, or there is no free variable importance. *Statistics and Computing* 2021; 31(6): 82. doi: [10.1007/s11222-021-10057-z](https://doi.org/10.1007/s11222-021-10057-z)
64. Watson DS, Wright MN. Testing conditional independence in supervised learning algorithms. *Machine Learning* 2021; 110(8): 2107–2129. doi: <https://doi.org/10.1007/s10994-021-06030-6>
65. Blesch K, Watson DS, Wright MN. Conditional feature importance for mixed data. *ASta Advances in Statistical Analysis* 2023: 1–20. doi: <https://doi.org/10.1007/s10182-023-00477-9>
66. Fisher A, Rudin C, Dominici F. All models are wrong, but many are useful: Learning a variable's importance by studying an entire class of prediction models simultaneously. *Journal of Machine Learning Research* 2019; 20(177): 1–81.
67. Altmann A, Toloşi L, Sander O, Lengauer T. Permutation importance: A corrected feature importance measure. *Bioinformatics* 2010; 26(10): 1340–1347. doi: <https://doi.org/10.1093/bioinformatics/btq134>
68. Hooker G. Discovering additive structure in black box functions. In: *KDD '04. Association for Computing Machinery*; 2004; New York, NY, USA: 575–580
69. Hooker G. Generalized functional anova diagnostics for high-dimensional functions of dependent variables. *Journal of Computational and Graphical Statistics* 2007; 16(3): 709–732. doi: [10.1198/106186007X237892](https://doi.org/10.1198/106186007X237892)
70. Hiabu M, Meyer JT, Wright MN. Unifying local and global model explanations by functional decomposition of low dimensional structures. In: Ruiz F, Dy J, Meent v. dJW., eds. *Proceedings of The 26th International Conference on Artificial Intelligence and Statistics*. 206 of *Proceedings of Machine Learning Research*. PMLR; 2023: 7040–7060.
71. Hastie T, Tibshirani R. Generalized Additive Models. *Statistical Science* 1986; 1(3): 297 – 310. doi: [10.1214/ss/1177013604](https://doi.org/10.1214/ss/1177013604)
72. Hastie T, Tibshirani R. Generalized additive models for medical research. *Statistical Methods in Medical Research* 1995; 4(3): 187–196. doi: [10.1177/096228029500400302](https://doi.org/10.1177/096228029500400302)
73. Bender A, Groll A, Scheipl F. A generalized additive model approach to time-to-event analysis. *Statistical Modelling* 2018; 18(3-4): 299-321. doi: [10.1177/1471082X17748083](https://doi.org/10.1177/1471082X17748083)
74. Tsai CP, Yeh CK, Ravikumar P. Faith-Shap: The faithful shapley interaction index. *Journal of Machine Learning Research* 2023; 24(94): 1–42. doi: <https://doi.org/10.48550/arXiv.2203.00870>
75. Olah C, Mordvintsev A, Schubert L. Feature visualization. *Distill* 2017; 2(11): e7.
76. Bau D, Zhou B, Khosla A, Oliva A, Torralba A. Network dissection: Quantifying interpretability of deep visual representations. In: *IEEE Computer Society*; 2017; Los Alamitos, CA, USA: 3319-3327
77. Zhong Y, She Y, Deng J, et al. Deep Learning for prediction of N2 metastasis and survival for clinical stage I non–small cell lung cancer. *Radiology* 2022; 302(1): 200-211. doi: [10.1148/radiol.2021210902](https://doi.org/10.1148/radiol.2021210902)
78. Banerjee M, Ding Y, Noone AM. Identifying representative trees from ensembles. *Statistics in Medicine* 2012; 31(15): 1601–1616. doi: <https://doi.org/10.1002/sim.4492>
79. Laabs BH, Westenberger A, König IR. Identification of representative trees in random forests based on a new tree-based distance measure. *Advances in Data Analysis and Classification* 2023: 1–18. doi: <https://doi.org/10.1007/s11634-023-00537-7>
80. Kalbfleisch JD, Prentice RL. *The Statistical Analysis of Failure Time Data*. John Wiley & Sons . 2002

81. Xie Y, Yu Z. Mixture cure rate models with neural network estimated nonparametric components. *Computational Statistics* 2021; 36(4): 2467–2489. doi: <https://doi.org/10.1007/s00180-021-01086-3>
82. Pölsterl S, Sarasua I, Gutiérrez-Becker B, Wachinger C. A wide and deep neural network for survival analysis from anatomical shape and tabular clinical data. In: Cellier P, Driessens K., eds. *Machine Learning and Knowledge Discovery in Databases* Springer International Publishing; 2020; Cham: 453–464
83. Wu J, Witten D. Flexible and interpretable models for survival data. *Journal of Computational and Graphical Statistics* 2019; 28(4): 954–966. doi: 10.1080/10618600.2019.1592758
84. Van Belle V, Pelckmans K, Suykens JA, Van Huffel S. Additive survival least-squares support vector machines. *Statistics in Medicine* 2010; 29(2): 296–308. doi: 10.1002/sim.3743
85. Rahman MM, Purushotham S. Fair and interpretable models for survival analysis. In: KDD '22. ; 2022; New York, NY, USA: 1452–1462
86. Agarwal R, Melnick L, Frosst N, et al. Neural additive models: Interpretable machine learning with neural nets. In: . 34. ; 2021: 4699–4711
87. Kopper P, Wiegrebe S, Bischl B, Bender A, Rügamer D. DeepPAMM: Deep piecewise exponential additive mixed models for complex hazard structures in survival analysis. In: Springer International Publishing; 2022; Cham: 249–261
88. Chen GH. Survival Kernets: Scalable and interpretable deep kernel survival analysis with an accuracy guarantee.; 2023
89. Kpotufe S, Verma N. Time-accuracy tradeoffs in kernel prediction: controlling prediction quality. *Journal of Machine Learning Research* 2017; 18: 1443–1471.
90. Zhao L, Dong Q, Luo C, et al. DeepOmix: A scalable and interpretable multi-omics deep learning framework and application in cancer survival analysis. *Computational and Structural Biotechnology Journal* 2021; 19: 2719–2725. doi: <https://doi.org/10.1016/j.csbj.2021.04.067>
91. Ching T, Zhu X, Garmire LX. Cox-nnet: An artificial neural network method for prognosis prediction of high-throughput omics data. *PLOS Computational Biology* 2018; 14(4): 1–18. doi: 10.1371/journal.pcbi.1006076
92. Wang Z, Sun J. SurvTRACE: Transformers for survival analysis with competing events. In: BCB '22. Association for Computing Machinery; 2022; New York, NY, USA
93. Groha S, Schmon SM, Gusev A. A general framework for survival analysis and multi-state modelling.; 2021.
94. Ghana Statistical Service (GSS) [Ghana] Ghana Health Service (GHS) [Ghana] and ICF International. *Ghana Demographic and Health Survey 2014 [Dataset]*. *GHBR72FL.SAS7BDAT*. 2015; Rockville, Maryland, USA: GSS, GHS, and ICF International [Distributor].
95. Spytek M, Krzyżiński M, Langbein SH, Baniecki H, Wright MN, Biecek P. survex: an R package for explaining machine learning survival models. *Bioinformatics* 2023; 39(12): btad723.
96. Molnar C, Casalicchio G, Bischl B. Interpretable machine learning—a brief history, state-of-the-art and challenges. In: Springer. ; 2020: 417–431.

A | APPENDIX

Name	Type	Description	Values
sex	cat	Sex of the child at birth	male (4078), female (3656)
place_residence	cat	Type of place of residence where the household resides	urban (3002); rural (4732)
wealth_idx	cat	Composite measure of a household's cumulative living standard	poorest (2635); poorer (1728); middle (1429); richer (1077); richest (865)
mother_age	num	Current age of the mother at time of questionnaire	15-49
age_head	num	Age of the head of household at time of questionnaire	16 - 95
total_dead_sons	num	Total number of sons who have died	0 - 5
total_dead_daughters	num	Total number of daughters who have died	0 - 5
multiples	cat	Order number for each child of a multiple birth	single child (7293); firstborn child (208); secondborn multiple (231); thirdborn multiple (2)
total_births_5years	num	Total number of births in the last five years	0 - 5
total_children	num	Total number of living children including current pregnancy	0 - 6
place_of_delivery	cat	Place of delivery of the child	home delivery (2419); public/government facility (4847); private facility (468); other (0)
dpt1_vaccination	cat	DPT 1 vaccination status recorded for children below the age of 3 years	no vaccination (625); vaccination date on health card (4171); vaccination reported by mother (527); vaccination marked on health card without date (14); don't know (9); child older than 3 years (2388)

TABLE 1 Description of the features selected for modelling the under-5 year survival time of children from the DHS birth recode from Ghana in 2014. The feature type is either numerical (num) or categorical (cat). In the values column, for numerical features the observed ranges are given; for categorical features the different categories are denoted with their observed frequencies in brackets.

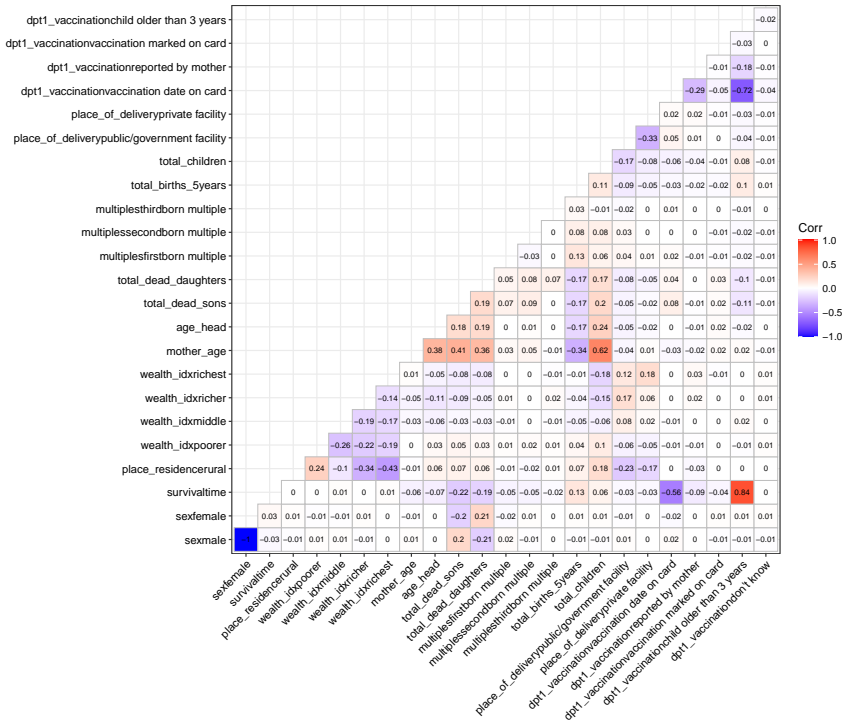


FIGURE 10 Correlations between features and survival time. Categorical features are one hot encoded for the purpose of computing the Pearson correlations.

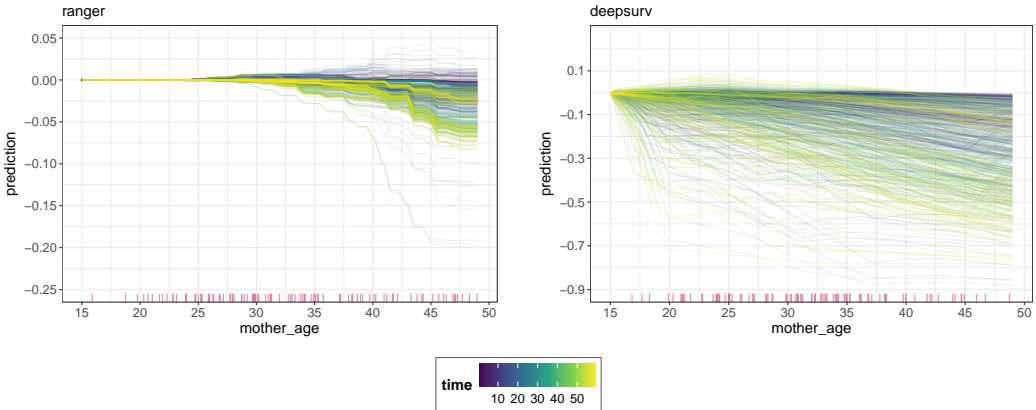


FIGURE 11 Centered ICE curves for the ranger model (left) and the deepsurv model (right) for the mother_age feature.

Individual	C1: Child dead at $t=0$	C2: Child censored at $t=23$
time	0	23
status	1	0
age_head	51	42
dpt1_vaccination	no	vaccination date on card
mother_age	43	18
multiples	secondborn multiple	single child
place_of_delivery	public/government facility	home delivery
place_residence	urban	rural
sex	female	female
total_births_5years	0	1
total_children	6	1
total_dead_daughters	2	0
total_dead_sons	0	0
wealth_idx	richer	poorest

TABLE 2 Observations used to compute *SurvLIME* and *SurvSHAP*(t) with corresponding feature values.

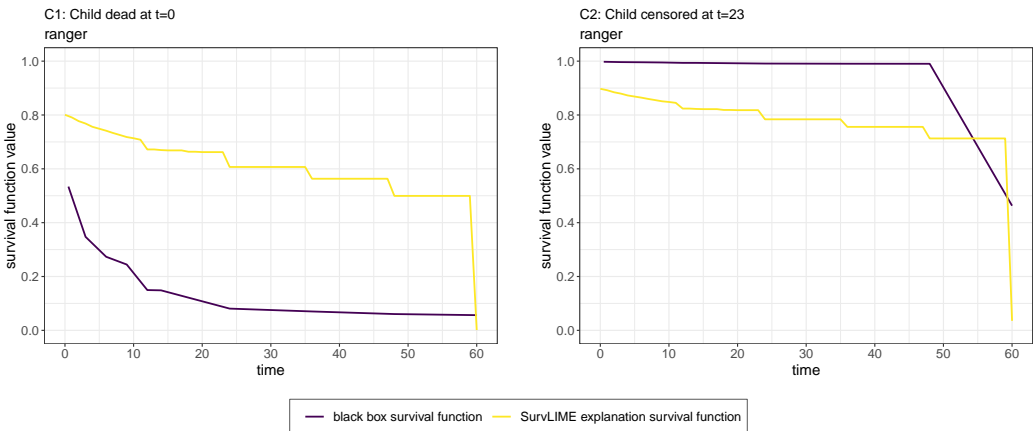


FIGURE 12 Black box survival functions predicted by the *ranger* model and *SurvLIME* explanation survival function for a child dead at $t = 0$ (left) and a child censored at $t = 23$.